EBM Experimental Biology and Medicine

TYPE Original Research
PUBLISHED 02 November 2026
DOI 10.3389/ebm.2026.11173

Check for updates

OPEN ACCESS

*CORRESPONDENCE
Jijin Yang,
jijinyang1@126.com

†These authors have contributed equally to this work

RECEIVED 01 May 2026
REVISED 16 September 2026
ACCEPTED 13 October 2026
PUBLISHED 02 November 2026

CITATION
Liu H, Wang F, Tian J, Luo R, Zhang J, Jiang X and Yang J (2026) Independent associations of gluteofemoral fat depots with hepatocellular carcinoma and the mediating role of the plasma lipidome: a mendelian randomization study. *Exp. Biol. Med.* 251:11173. doi: 10.3389/ebm.2026.11173

COPYRIGHT
© 2026 Liu, Wang, Tian, Luo, Zhang, Jiang and Yang. This is an open-access article distributed under the terms of the Creative Commons Attribution License (CC BY). The use, distribution or reproduction in other forums is permitted, provided the original author(s) and the copyright owner(s) are credited and that the original publication in this journal is cited, in accordance with accepted academic practice. No use, distribution or reproduction is permitted which does not comply with these terms.

Independent associations of gluteofemoral fat depots with hepatocellular carcinoma and the mediating role of the plasma lipidome: a mendelian randomization study

Hang Liu[1†], Fuming Wang[1,2†], Jinming Tian[1,3†], Rong Luo[1], Jianan Zhang[1], Xu Jiang[1] and Jijin Yang[1*]

[1]Department of Interventional Therapy, Changhai Hospital, Navy Medical University, Shanghai, China, [2]Department of Cardiology and Nephrology, Hospital of the 72nd Group Army, PLA, Huzhou, Zhejiang, China, [3]Department of Nuclear Medicine, Changhai Hospital, Navy Medical University, Shanghai, China

Abstract

As metabolic etiologies become increasingly important in hepatocellular carcinoma (HCC), the causal roles of specific adipose depots independent of overall body size remain unclear. This study used Mendelian randomization (MR) to investigate the associations of MRI-derived fat-depot phenotypes with HCC and to explore potential mediation by plasma lipids. GWAS summary statistics for BMI- and height-adjusted fat-depot phenotypes were obtained from the UK Biobank, and HCC summary statistics were obtained from FinnGen, with replication in the Million Veteran Program. Univariable and multivariable MR were used to estimate total and independent effects, including analyses adjusted for smoking, alcohol consumption, type 2 diabetes, and childhood BMI. A two-step MR framework was applied to assess mediation by 179 plasma lipid species. Genetically predicted gluteofemoral adipose tissue adjusted for BMI and height (GFATadj) was associated with a lower risk of HCC (OR = 0.444, P = 1.00×10^{-4}). This association remained robust after adjustment for other risk factors, and it was replicated in the Million Veteran Program (OR = 0.766). Mediation analysis identified six lipid species as potential partial mediators, each accounting for an estimated 7.0%–15.4% of the protective total effect, and colocalization provided only limited support for shared causal variants. Our results provide insight into depot-specific adiposity and lipid metabolic pathways in hepatocarcinogenesis, although further validation is needed to confirm the underlying causal mechanisms.

KEYWORDS
gluteofemoral fat depots, hepatocellular carcinoma, mediation analysis, Mendelian randomization, plasma lipidome

Impact statement

This study identifies a protective role of gluteofemoral fat against hepatocellular carcinoma, offering new insights into how fat distribution influences cancer risk. By uncovering specific lipids that may mediate this effect, it highlights potential targets for prevention strategies. These findings advance understanding of adiposity and lipid metabolism in hepatocarcinogenesis, supporting the development of population-level interventions to reduce HCC risk.

Introduction

Hepatocellular carcinoma (HCC), the predominant histological subtype of primary liver cancer, remains a major global health challenge. In 2020, primary liver cancer was the sixth most commonly diagnosed malignancy and the third leading cause of cancer-related death worldwide, accounting for an estimated 906,000 new cases and 830,000 deaths [1]. Given its high mortality and the limited treatment options available for advanced disease, identifying modifiable risk factors for HCC is essential for improving prevention strategies.

Although chronic viral hepatitis remains a leading cause of HCC, the epidemiological landscape is increasingly shaped by non-viral metabolic risk factors. In particular, metabolic dysfunction-associated fatty liver disease (MAFLD) has emerged as an important contributor to HCC in the context of rising obesity, type 2 diabetes (T2D), and metabolic syndrome [2–4]. As a modifiable determinant closely linked to these metabolic abnormalities, obesity represents an important target for HCC prevention [5–7]. However, obesity is a heterogeneous phenotype, and its relationship with HCC risk may depend not only on overall adiposity but also on fat distribution.

Although body mass index (BMI) is widely used in studies of obesity-related cancer risk, it is a crude measure that does not capture biologically relevant differences in adipose tissue distribution [8, 9]. This limitation is important because distinct fat depots exert divergent metabolic effects. Visceral and upper-body adiposity are associated with insulin resistance, cardiovascular disease, and adverse metabolic outcomes, whereas gluteofemoral adiposity is linked to a more favorable cardiometabolic profile [10]. Accordingly, overall obesity and depot-specific adiposity should not be considered interchangeable, and reliance on BMI alone may obscure adiposity patterns that are more relevant to HCC risk [11].

Conventional anthropometric indices such as waist-to-hip ratio (WHR) provide only a limited representation of fat distribution [12]. An elevated WHR may arise from greater visceral or abdominal adiposity, lower gluteofemoral fat, or both, making it difficult to isolate the independent contribution of specific fat depots. Imaging approaches such as dual-energy X-ray absorptiometry (DEXA) and computed tomography (CT) offer more direct assessment of regional adiposity, and several studies suggest that central adiposity may be more strongly associated with primary liver cancer risk than BMI [13–15]. However, many prior imaging studies did not adequately account for height or overall body size and often lacked direct quantification of gluteofemoral fat [16, 17]. These limitations highlight the need for more refined phenotypes that separately capture visceral, abdominal subcutaneous, and gluteofemoral adiposity.

To address these methodological limitations, Agrawal et al. developed MRI-derived, body-size-independent adiposity phenotypes in 38,965 UK Biobank participants by quantifying visceral, abdominal subcutaneous, and gluteofemoral fat volumes and adjusting them for BMI and height [11]. The resulting traits, VATadj, ASATadj, and GFATadj, better isolate depot-specific adiposity than conventional anthropometric measures. These phenotypes have since been associated with several cardiometabolic and liver-related outcomes, including inverse associations of GFATadj with T2D and non-alcoholic fatty liver disease (NAFLD) [18]. However, whether these refined fat-depot phenotypes are causally associated with HCC risk remains unclear.

Beyond clarifying the relationship between depot-specific adiposity and HCC, it is also important to understand the biological pathways through which such effects may operate. Plasma lipids are plausible intermediates in this context because circulating lipid species reflect systemic and hepatic metabolic states, and accumulating evidence has highlighted a potential role for lipid metabolic dysregulation in hepatocarcinogenesis [19–22]. Lipidomic profiling therefore provides an opportunity to identify specific molecular intermediates that may link regional adiposity to HCC development.

In this study, we aimed to determine whether MRI-derived, depot-specific adiposity phenotypes are causally associated with HCC risk and whether specific plasma lipids mediate these associations. To this end, we applied univariable Mendelian randomization (UVMR), multivariable Mendelian randomization (MVMR), and a two-step MR framework to evaluate the total and independent effects of fat-depot phenotypes on HCC and to investigate potential lipid-mediated pathways linking regional adiposity to hepatocarcinogenesis [23].

Materials and methods

Study design

The study comprised two phases (Figure 1A). In phase 1, we used univariable Mendelian randomization (UVMR) to estimate the total effects of each fat-depot phenotype on hepatocellular carcinoma (HCC), and multivariable Mendelian randomization (MVMR) to assess their independent effects. To examine the robustness of these associations to related metabolic and behavioral risk factors, we performed a series of additional MVMR models that separately adjusted for smoking, alcohol consumption, childhood BMI, and type 2 diabetes [24].

In phase 2, we evaluated 179 plasma lipid species as candidate mediators linking fat-depot phenotypes to HCC (Figure 1B). We applied a prespecified four-step screening framework. First, we assessed the effects of fat-depot phenotypes on circulating lipids using UVMR. Second, we tested whether candidate lipids were independently associated with HCC after accounting for fat-depot phenotypes using MVMR. Third, we performed reverse MR analyses to exclude evidence of reverse causality. Finally, for lipids that satisfied these criteria, we quantified indirect effects using

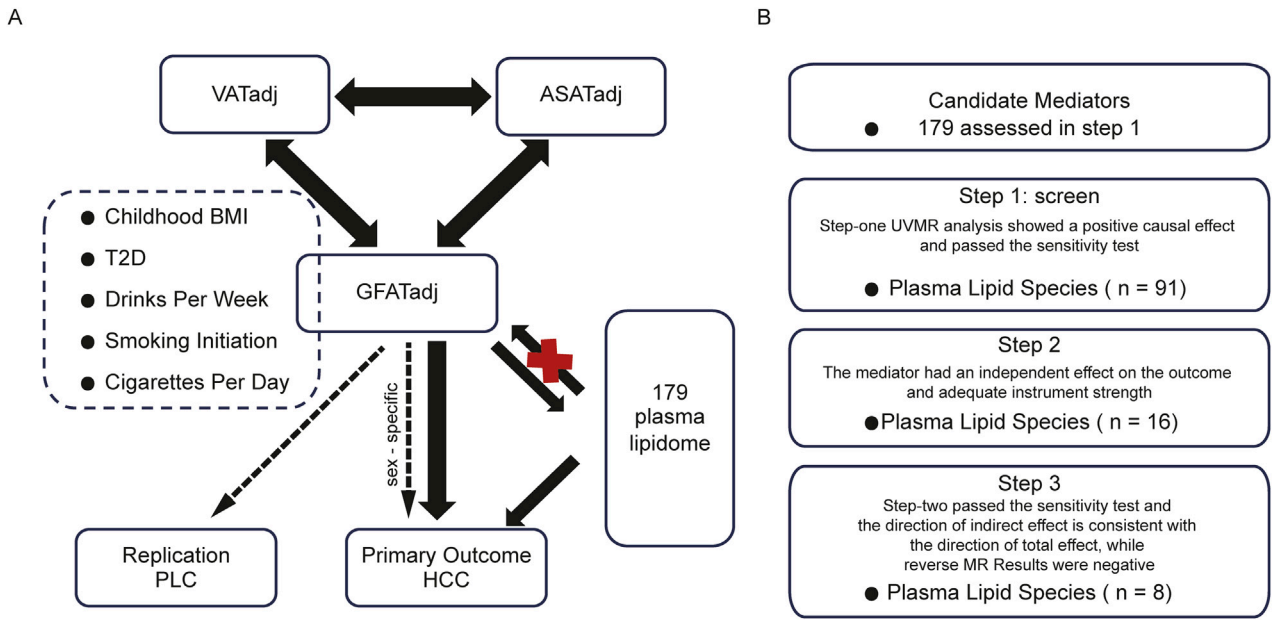


FIGURE 1
Overview of the study design. **(A)** Study design; **(B)** Mediator selection process. This study consisted of 2 stages of analyses. In stage 1, we assessed the causal associations of VATadj, GFATadj, and ASATadj with HCC (outcome) using UVMR and MVMR to evaluate the overall and independent causal effects of each exposure on outcomes, respectively. Furthermore, we assessed the causal associations of GFATadj, childhood BMI, T2D, Drinks per week, smoking initiation, and cigarettes per day with HCC (outcome) using MVMR to evaluate the independent causal effect of GFATadj and each confounder on outcomes, respectively. In stage 2, we first screened candidate mediators for the association between GFATadj and HCC by established criteria, and then calculated their mediating effects using 2-step MVMR. VATadj indicates visceral adipose tissue adjusted for BMI and height; GFATadj, gluteofemoral adipose tissue adjusted for BMI and height; ASATadj, abdominal subcutaneous adipose tissue adjusted for BMI and height; BMI, body mass index; T2D, type 2 diabetes.

a two-step MR mediation framework. Only lipids that passed this sequential screening strategy were considered putative mediators.

This study is reported in accordance with the STROBE-MR guidelines (STROBE-MR) [25], and the completed checklist is provided in the Supplementary Material.

Data sources

Summary-level GWAS data for exposures, outcomes, mediators, and related risk factors were obtained from publicly available studies. To minimize bias from population stratification, all analyses were restricted to individuals of European ancestry. Detailed characteristics of each dataset are summarized in Table 1. Because only publicly available summary statistics were used, no additional ethical approval was required.

Fat-depot phenotypes

MRI-derived fat-depot phenotype summary statistics from Agrawal et al. [11] were derived from 38,965 UK Biobank participants after quality control of an initial 39,076 genotyped individuals; all subsequent analyses herein are based on these summary statistics. The phenotypes included visceral adipose tissue adjusted for BMI and height (VATadj), abdominal subcutaneous adipose tissue adjusted for BMI and height (ASATadj), and gluteofemoral adipose tissue adjusted for BMI and height (GFATadj). In the source GWAS, the adjusted traits were constructed as residualized fat-depot measures after regression on relevant covariates, including BMI and height, and were analyzed on inverse-normal transformed scales. Although adjustment for BMI and height may in principle raise concerns about collider bias, empirical evidence from the original GWAS suggests that substantial collider bias is unlikely. Specifically, these adjusted phenotypes showed low genetic correlations with BMI and height, most associated loci had larger effects on the corresponding unadjusted fat depots than on BMI or height, and polygenic scores derived from these traits were strongly related to fat depots but minimally related to BMI or height. [11]. Additionally, sex-specific exposure summary statistics were used in exploratory analyses. Because sex-specific outcome data were unavailable, these analyses applied sex-specific exposure instruments to a combined-sex HCC outcome.

Outcome datasets

HCC summary statistics for the primary analysis were obtained from FinnGen [26], including 500 cases defined by ICD-10 code C22.0 and 314,193 controls. For replication, we used summary statistics for primary liver cancer from the Million Veteran Program (MVP) [27, 28], comprising 2,852 cases and 447,587 controls. In MVP, cases were identified using PheCode 155.1, which may introduce some phenotypic heterogeneity relative to the discovery-stage HCC definition.

Plasma lipidome

Summary statistics for 179 plasma lipid species used as candidate mediators were obtained from Ottensmann et al. [29].

TABLE 1 Summary of GWAS datasets used in the study.

Traits	Sources	N	Ancestry	PMID	PY
Exposure					
VATadj	https://personal.broadinstitute.org/ryank/Agrawal_2022_Fat_Depots_GWAS.zip	38,965	European	35773277	2022
GFATadj	https://personal.broadinstitute.org/ryank/Agrawal_2022_Fat_Depots_GWAS.zip	38,965	European	35773277	2022
ASATadj	https://personal.broadinstitute.org/ryank/Agrawal_2022_Fat_Depots_GWAS.zip	38,965	European	35773277	2022
Sex-stratified exposure					
GFATadj_Male	https://personal.broadinstitute.org/ryank/Agrawal_2022_Fat_Depots_GWAS.zip	19,089	European	35773277	2022
GFATadj_Female	https://personal.broadinstitute.org/ryank/Agrawal_2022_Fat_Depots_GWAS.zip	19,867	European	35773277	2022
Outcome					
HCC	https://storage.googleapis.com/finngen-public-data-r10/summary_stats/finngen_R10_C3_HEPATOCELLU_CARC_EXALLC.gz	314,693	European	NA	2024
PLC	https://www.ebi.ac.uk/gwas/studies/GCST90475569	450,439	European	39024449	2024
Confounders					
SmokingInitiation	https://conservancy.umn.edu/handle/11299/201564	175,189	European	30643251	2019
CigarettesPerDay	https://conservancy.umn.edu/handle/11299/201565	106,780	European	30643251	2019
DrinksPerWeek	https://conservancy.umn.edu/handle/11299/201566	168,179	European	30643251	2019
Childhood BMI	https://www.ebi.ac.uk/gwas/publications/33045005	39,620	European	33045005	2020
T2D	https://cnsgenomics.com/content/data	659,316	European	30054458	2018
Candidate mediators					
Plasma lipidomics GCST90277238-GCST90277416	https://www.ebi.ac.uk/gwas/downloads/summary-statistics	7,174	European	37907536	2023

In that study, shotgun lipidomics was performed in 7,174 Finnish individuals, quantifying lipids across 13 subclasses, including glycerolipids, glycerophospholipids, sphingolipids, and sterols. In the source GWAS, measured lipid levels were adjusted for relevant covariates, including age, sex, collection site, lipid medication, genetic principal components, and ancestry, and the resulting residuals were inverse-normal transformed before association testing. Therefore, the corresponding genetic effect estimates should be interpreted on standardized transformed-trait scales rather than as effects on raw lipid concentrations.

Related risk factors

Genetic instruments for prespecified behavioral and metabolic risk factors were obtained from large-scale GWAS meta-analyses, including smoking and alcohol traits (N ranged from 106,780 to 175,189; excluding UK Biobank and 23andMe to reduce sample overlap) [30], childhood BMI (N = 39,620) [31], and Type 2 Diabetes (62,892 cases, 596,424 controls) [32].

Selection of instrumental variables

Instrumental variables (IVs) were selected from SNPs associated with each exposure at genome-wide significance ($P < 5 \times 10^{-8}$) and clumped for independence using a linkage disequilibrium threshold of $r^2 < 0.001$ within a 10,000-kb window. When an exposure SNP was unavailable in the outcome dataset, proxy SNPs in high linkage disequilibrium ($r^2 > 0.8$) were identified using the LDlinkR package. Exposure and outcome datasets were harmonized to align effect alleles, and missing allele frequencies were inferred from the 1000 Genomes Phase 3 reference panel [33].

For analyses involving the primary fat-depot exposures, IVs were selected using the genome-wide significance threshold described above. For lipid mediator analyses, however, the SNP selection threshold was relaxed to $P < 5 \times 10^{-6}$ to ensure a sufficient number of instruments for multivariable MR, consistent with previous MR studies [34, 35]. To reduce the risk of weak instrument bias associated with this more lenient threshold, instrument strength was subsequently evaluated using F-statistics and conditional F-statistics, and only mediators with adequate instrument strength were retained for downstream analyses.

Instrument strength was assessed by calculating the proportion of phenotypic variance explained (R^2) and the corresponding F-statistic [36]:

$$F = \frac{R^2}{1 - R^2} * \frac{N - K - 1}{K}$$

where N is the sample size, K is the number of SNPs, and R^2 represents the variance explained by the IVs. R^2 was calculated as:

$$R^2 = \frac{2*\beta^2*EAF*(1-EAF)}{2*\beta^2*EAF*(1-EAF) + 2*SE^2*N*EAF*(1-EAF)}$$

where β, SE, EAF, and N denote the effect size, standard error, effect allele frequency, and total sample size of the exposure phenotype data, respectively [37]. An F-statistic >10 was considered indicative of adequate instrument strength. For MVMR analyses, instrument strength was further evaluated using conditional F-statistics, with the same threshold applied [38, 39]. Statistical power was estimated using the online tool[1] based on the method described by Burgess et al. [40].

Detailed information on the selected IVs, including rsID, chromosome position, effect estimates, standard errors, P values, and F-statistics, is provided in the Supplementary Tables S1–S7, S10, S12–S18, S23, S26, S30, S33.

Statistical analysis

Unless otherwise specified, effect estimates for adipose-depot phenotypes and lipid mediators were interpreted on the standardized trait scales used in the source GWAS. For HCC-related analyses, causal estimates were reported on the odds ratio scale, and mediation effects were estimated on the log-odds scale and additionally presented as odds ratios where appropriate.

Mendelian randomization and sensitivity analysis

Univariable Mendelian randomization (MR) analyses were primarily conducted using the inverse-variance weighted (IVW) method [41]. Weighted median and MR-Egger regression were used as complementary estimators to assess the robustness of the primary findings [42, 43]. All MR analyses were interpreted under the standard assumptions of relevance, independence, and exclusion restriction [44], and non-overlapping datasets were prioritized where possible to reduce potential bias.

Heterogeneity was assessed using Cochran's Q statistic, and directional horizontal pleiotropy was evaluated using the MR-Egger intercept test. A Q-statistic with $P < 0.05$ was considered to indicate heterogeneity, whereas an MR-Egger intercept significantly different from zero was considered evidence of directional pleiotropy [42, 45].

Global pleiotropy and influential outliers were further assessed using the MR-PRESSO global test and the RadialMR framework with modified second-order weights [46, 47]. When evidence of outlier-driven distortion was identified, influential SNPs were removed and causal estimates were re-evaluated. Outlier significance was assessed using a Bonferroni-corrected threshold based on the number of instruments tested. Funnel plots, leave-one-out analyses, and radial plots were used for visual assessment of instrument influence and estimate stability [45].

Multivariable MR and mediation analysis

We used a prespecified two-step MR mediation framework to evaluate whether plasma lipids mediated the associations between fat-depot phenotypes and HCC [48]. In step 1, UVMR was used to estimate the effects of fat-depot phenotypes on candidate lipid mediators. In step 2, MVMR was used to estimate the direct effects of lipid mediators on HCC while adjusting for the corresponding fat-depot phenotype [49, 50].

Candidate mediators were selected according to the four-step screening framework outlined in the Study Design section. In step 1, lipid candidates were retained if the IVW analysis showed nominal evidence of association ($P < 0.05$), the weighted median and MR-Egger estimates were directionally concordant, and there was no substantial evidence of horizontal pleiotropy. For associations showing heterogeneity, RadialMR was applied to identify and remove influential outliers before final evaluation. In step 2, candidate lipids were required to show an independent association with HCC in MVMR and adequate instrument strength (conditional F-statistic >10). In step 3, reverse MR analyses were performed, and lipids showing evidence of reverse causality were excluded. In step 4, indirect effects were estimated only for lipids meeting the above criteria, and mediators were retained if the indirect effect was statistically significant and directionally consistent with the total effect.

Indirect effects were estimated by the product-of-coefficients method. Standard errors and 95% confidence intervals were obtained from the distribution of the product of the two component estimates (RMediation::medci, type = "dop", alpha = 0.05, rho = 0) [51], equivalent to the PRODCLIN approach [52], with the product CDF evaluated by the Meeker–Escobar algorithm [53]. The standard errors are the exact standard errors of the product of two normal random variables [54], $\mathrm{Var}(\beta_1\beta_2) = \beta_1^2\mathrm{Var}(\beta_2) + \beta_2^2\mathrm{Var}(\beta_1) + 2\beta_1\beta_2\mathrm{Cov}(\beta_1,\beta_2) + \mathrm{Var}(\beta_1)\mathrm{Var}(\beta_2)(1+\rho^2)$, where ρ is the correlation between the two component estimates; the covariance term vanishes at $\rho = 0$ and the final term is the higher-order term omitted by the first-order Delta method. With $\rho = 0$ the standard error reduces to $\sqrt{(\beta_1^2SE_2^2 + \beta_2^2SE_1^2 + SE_1^2SE_2^2)}$, which is the form used here. Because the same lipid GWAS supplies both steps of the design, the correlation between them was quantified from shared SNP-level data, analytically and by Monte Carlo simulation, and the indirect effects were examined across ρ values from −0.99 to 0.99 (step 0.01) using the same distribution-of-the-product method. Confidence limits are the 2.5th and 97.5th percentiles of the product distribution, which, because the distribution of the product of two variables with non-zero means is skewed, are not necessarily symmetric.

Two-sided P values were obtained by Monte Carlo evaluation of the same product distribution (1×10^6 draws) as twice the smaller tail probability at zero, and were then subjected to Benjamini–Hochberg FDR correction (Section *Correction for multiple testing*). Mediation proportions were calculated as the ratio of the indirect effect to the total effect of GFATadj on HCC, estimated by inverse-variance weighted MR.

The two-step MR mediation framework was interpreted under several assumptions: the genetic instruments were relevant for the exposure and, where applicable, for the mediator; instrument–outcome associations operated through the hypothesized exposure–mediator–outcome pathway rather than through alternative pleiotropic pathways; and the causal direction was

1 https://sb452.shinyapps.io/power/

correctly specified. Consistent with standard summary-data MR mediation analyses, we assumed linear and additive effects on the log-odds scale and no important exposure–mediator interaction. To assess the plausibility of these assumptions, we evaluated instrument strength using F-statistics, examined reverse causality using bidirectional MR, and performed robust MVMR analyses using MVMR-Egger, MVMR-Median, and MVMR-Robust methods [55].

As an additional locus-level analysis, Bayesian colocalization was performed to assess whether prioritized mediator–outcome associations were consistent with shared causal variants rather than linkage disequilibrium [56]. For each prioritized signal, summary statistics for all SNPs within 250 kb of the lead SNP were extracted, and PP.H4 > 0.80 was considered supportive evidence for colocalization.

Correction for multiple testing

To control for multiple testing, Benjamini–Hochberg false discovery rate (FDR) correction was applied separately within three prespecified hypothesis families [57]: (1) the effects of fat-depot phenotypes on HCC; (2) the effects of fat-depot phenotypes on plasma lipid mediators; and (3) the independent effects of plasma lipid mediators on HCC. In addition, a fourth family was defined for the formal mediation tests: (4) the indirect (mediation) effects of GFATadj on HCC acting through plasma lipid mediators. Associations with $P < 0.05$ and FDR-adjusted $q < 0.05$ were considered FDR-significant, whereas associations with $P < 0.05$ that did not survive FDR correction were considered nominally significant (suggestive evidence). The mediator-screening stage (family 2) was designed as an exploratory step. Nominal significance was used as a deliberately sensitive initial filter, to avoid excluding potential true mediators at this stage, and the Benjamini–Hochberg FDR-adjusted values reported for this family are descriptive.

Statistical software

All statistical analyses were performed using R version 4.3.1 (R Foundation for Statistical Computing, Vienna, Austria). MR and MVMR analyses were conducted primarily using the TwoSampleMR (v0.6.8), MVMR (v0.4), and MendelianRandomization (v0.9.0) packages. Outlier and pleiotropy assessments were performed using MRPRESSO (v1.0) and RadialMR (v1.1), and data processing for genetic instruments was supported by ieugwasr (v1.0.2) and LDlinkR (v1.4.0). Bayesian colocalization analyses were performed using the coloc (v5.2.3). Figures were generated using ggplot2 (v3.4.2). Multiple-testing correction was implemented in R using the p.adjust() function with method = "fdr", corresponding to the Benjamini–Hochberg procedure. To ensure reproducibility, detailed R session information and analytic scripts are available in a public GitHub repository.[2]

2 https://github.com/luanshifusheng91/Mendelian-Project

Results

UVMR and MVMR assessments of the independent and total effects of fat-depot phenotypes on HCC

Characteristics and strength of genetic instruments

We first assessed the genetic instruments for the three fat-depot phenotypes. After quality control, 18, 35, and 18 SNPs were retained as instrumental variables for VATadj, GFATadj, and ASATadj, respectively (Supplementary Table S1). Across the three traits, the instruments explained 1.84%–4.72% of phenotypic variance, and all mean F-statistics exceeded the conventional threshold of 10 (VATadj, 49.3; GFATadj, 55.3; ASATadj, 40.7). Statistical power was high for GFATadj (97.6%) but low for VATadj and ASATadj (3.1% and 5.2%, respectively).

In the MVMR analyses, conditional F-statistics after mutual adjustment were 13.01 for GFATadj, 12.53 for VATadj, and 15.57 for ASATadj (Supplementary Table S2). The additionally adjusted behavioral and metabolic risk factors also showed adequate instrument strength, with conditional F-statistics ranging from 11.52 to 47.10 (Supplementary Tables S3–S8).

Primary MR analysis results

In UVMR, genetically predicted GFATadj was inversely associated with HCC risk (IVW-OR = 0.444, 95% CI 0.294–0.669, $P = 1.00 \times 10^{-4}$, FDR-adjusted $q = 3.00 \times 10^{-4}$), whereas VATadj and ASATadj showed no significant associations (Figure 2). The univariable MR estimates for ASATadj and VATadj use all genome-wide significant instruments. When primary analyses showed heterogeneity and outlier-driven pleiotropy, results after outlier removal are presented as sensitivity analyses (Supplementary Figure S1).

In MVMR adjusting for VATadj and ASATadj, GFATadj remained inversely associated with HCC (IVW-OR = 0.455, 95% CI 0.261–0.793, $P = 0.0054$), as shown in Figure 2. Additional MVMR models adjusting separately for smoking traits, alcohol intake, childhood BMI, and T2D showed similar estimates, with ORs ranging from 0.40 to 0.44 across models (Figure 3).

Sensitivity analyses

Sensitivity analyses supported the robustness of the UVMR findings. For GFATadj and VATadj, neither Cochran's Q test nor the MR-PRESSO global test indicated significant heterogeneity, and the MR-Egger intercept test showed no evidence of directional pleiotropy (Supplementary Table S9).

In contrast, ASATadj showed evidence of heterogeneity (Cochran's Q = 40.7, Q_df = 17, Q_P = 0.001) and outlier-driven pleiotropy (MRPRESSO_P = 0.002) (Supplementary Table S9). RadialMR identified five outlier SNPs (rs1159619,

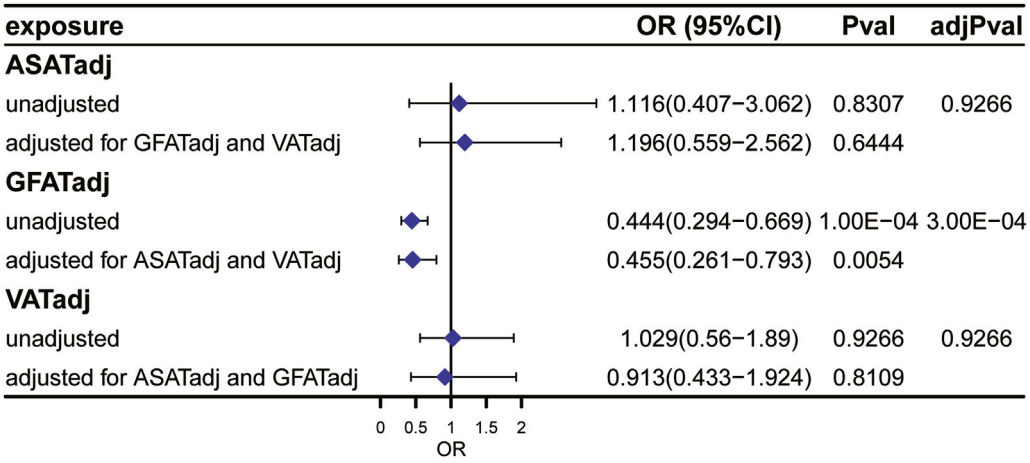


FIGURE 2
UVMR and MVMR estimates of the causal associations of VATadj, GFATadj, and ASATadj with HCC. Plots (bars) represent OR (95% CI). OR indicates odds ratio; VATadj indicates visceral adipose tissue adjusted for BMI and height; GFATadj, gluteofemoral adipose tissue adjusted for BMI and height; ASATadj, abdominal subcutaneous adipose tissue adjusted for BMI and height; UVMR, univariable Mendelian randomization; MVMR, multivariable Mendelian randomization; and adjPval was calculated by Benjamini-Hochberg method.

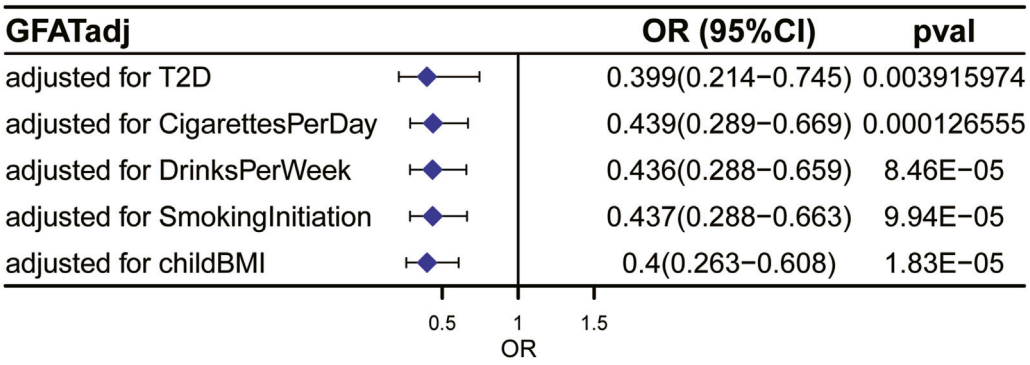


FIGURE 3
MVMR estimates of the causal associations of GFATadj and each confounder with HCC. Plots (bars) represent OR (95% CI). OR indicates odds ratio; T2D, type 2 diabetes; and MVMR, multivariable Mendelian randomization.

rs2943647, rs3850625, rs7538503, and rs7649153) (Supplementary Table S10). After excluding these variants, heterogeneity was no longer evident (Cochran's Q = 10.8, Q_df = 12, Q_*P* = 0.545, MRPRESSO_*P* = 0.553) (Supplementary Table S11). The re-estimated causal effect for ASATadj remained directionally consistent with the primary analysis (IVW OR = 1.174, 95% CI 0.539–2.553, P = 0.6866, FDR-adjusted q = 0.8239) and remained non-significant (Supplementary Figure S1).

Funnel plots showed general symmetry for GFATadj and the corrected ASATadj instruments (Supplementary Material 1). Slight asymmetry was observed for VATadj, although the MR-Egger intercept remained non-significant. Leave-one-out analyses indicated that the association between GFATadj and HCC was not driven by any single SNP, whereas omission of individual SNPs for VATadj and ASATadj led to some fluctuation in effect estimates but confidence intervals consistently crossed the null (Supplementary Material 1). Radial plots showed close alignment of GFATadj instruments with the regression lines, whereas greater separation between the IVW and MR-Egger lines was observed for VATadj and ASATadj (Supplementary Material 1).

Replication analysis

In the replication analysis using PLC from the Million Veteran Program, 19, 38, and 18 SNPs were retained as instruments for VATadj, GFATadj, and ASATadj, respectively, explaining 1.84%–5.14% of phenotypic variance (Supplementary Table S1). Statistical power for the associations with primary liver cancer (PLC) was 10.6% for VATadj, 89.6% for GFATadj, and 63.0% for ASATadj.

In the replication analysis, genetically predicted GFATadj was inversely associated with PLC risk (IVW-OR = 0.766, 95% CI 0.631–0.923, *P* = 0.0068; FDR-adjusted *q* = 0.02), whereas VATadj and ASATadj showed no significant associations (Supplementary Figure

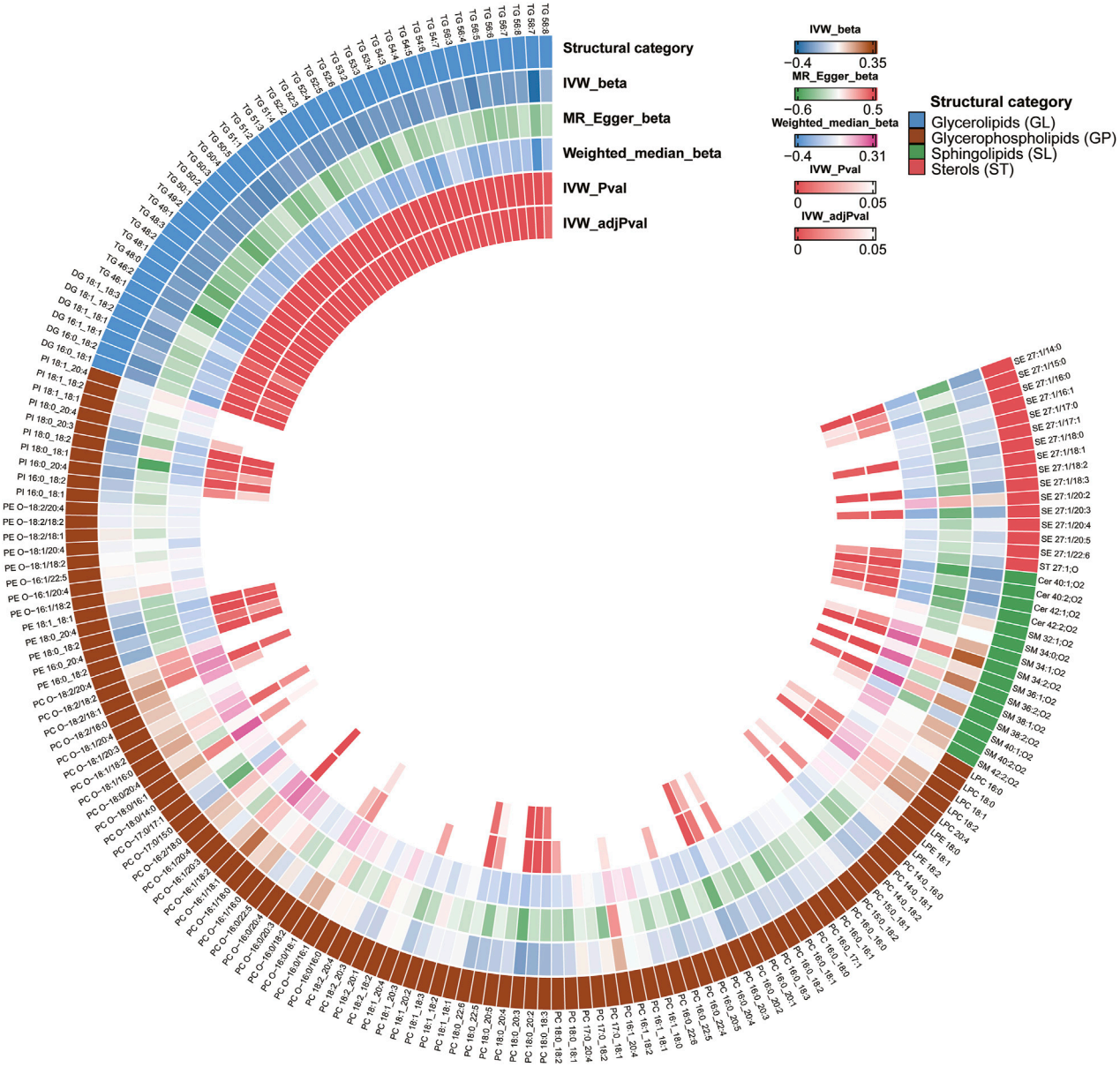


FIGURE 4
Step one UVMR of Two-step Mendelian randomization estimates of the causal associations of GFATadj with each plasma lipid. Plot showing the effect (beta) of GFATadj on the mediators (univariable MR) from IVW, MR-Egger, and weighted median analyses. IVW-adjusted P values were calculated using the Benjamini-Hochberg method. For the 27 lipid outcomes flagged for heterogeneity or outlier-driven pleiotropy, estimates are those obtained after RadialMR outlier removal.

S1). Sensitivity analyses for GFATadj showed no evidence of heterogeneity (Cochran's Q = 45.3, Q_*P* = 0.163), directional pleiotropy (MR-Egger intercept *P* = 0.147), or global pleiotropy (MR-PRESSO global test *P* = 0.146) (Supplementary Table S3). Leave-one-out analyses and scatter plots also showed no evidence that the result was driven by a single SNP (Supplementary Material 1).

In replication-stage MVMR analyses, conditional F-statistics for all exposures were greater than 10 (Supplementary Tables S8, S12–S17). GFATadj remained inversely associated with PLC after additional adjustment for smoking initiation, cigarette consumption, alcohol intake, childhood BMI, and T2D, with ORs ranging from 0.681 to 0.783 across models (Supplementary Figure S2).

Exploratory sex-stratified analysis

Because sex-specific outcome summary statistics were unavailable, sex-specific GFATadj instruments were analysed against the combined-sex HCC outcome, making these analyses exploratory by design. The inverse-variance weighted estimates were directionally consistent in both strata (male-specific OR = 0.328, 95% CI 0.167–0.643; female-specific OR = 0.528, 95% CI 0.348–0.801), with no

evidence of heterogeneity or directional pleiotropy in either stratum (Supplementary Tables S18–S20).

Two-step MR investigates the relationship between GFATadj, lipidomics, and HCC

Characteristics of genetic instruments in two-step MR

In the step-one UVMR analyses, GFATadj was used as the exposure across all 179 plasma lipid outcomes. The corresponding genetic instrument comprised 34 SNPs, explaining 4.64% of the phenotypic variance, with an F-statistic of 50.8 (Supplementary Table S21).

In the step-two MVMR analyses, we evaluated candidate lipid mediators carried forward from step one. Across these models, the conditional F-statistics for GFATadj ranged from 26.4 to 44.6, whereas those for the included lipid exposures ranged from 4.3 to 29.4 (Supplementary Table S22). Lipid candidates with insufficient conditional instrument strength were subsequently excluded from downstream mediation analyses (Supplementary Table S23).

Results of step-one MR analysis: GFATadj and plasma lipidome

The primary step-one IVW analysis showed broad associations between genetically predicted GFATadj and the plasma lipidome (Figure 4). Overall, GFATadj was associated with lower levels of several neutral and storage-related lipid classes, whereas phospholipid changes were more subclass-specific, with positive associations observed for lysophosphatidylcholines, sphingomyelins, and selected ether-linked phosphatidylcholines (Supplementary Table S24).

Among neutral and storage-related lipids, triglyceride and diglyceride species were predominantly inversely associated with GFATadj. Representative associations included TG 58:7 ($\beta = -0.396$, FDR-adjusted $q = 4.53 \times 10^{-6}$), TG 56:4 ($\beta = -0.304$, FDR-adjusted $q = 2.26 \times 10^{-4}$), DG 18:1_18:2 ($\beta = -0.258$, FDR-adjusted $q = 1.17 \times 10^{-3}$) and DG 18:1_18:1 ($\beta = -0.246$, FDR-adjusted $q = 1.76 \times 10^{-3}$). Inverse associations were also observed for several ceramide species, sterol esters, and free cholesterol, including Cer d40:1 ($\beta = -0.258$, FDR-adjusted $q = 1.31 \times 10^{-4}$), SE 27:1/14:0 ($\beta = -0.232$, FDR-adjusted $q = 3.72 \times 10^{-4}$), and cholesterol ($\beta = -0.151$, FDR-adjusted $q = 0.023$) (Supplementary Table S24).

Phospholipid associations varied by subclass. Lysophosphatidylcholines were positively associated with GFATadj, as illustrated by LPC 20:4 ($\beta = 0.193$, FDR-adjusted $q = 0.006$) and LPC 18:1 ($\beta = 0.135$, FDR-adjusted $q = 0.034$). By contrast, several diacyl phosphatidylcholines, phosphatidylethanolamines, and phosphatidylinositols were inversely associated, including PC 18:0_20:3 ($\beta = -0.256$, FDR-adjusted $q = 3.72 \times 10^{-4}$), PE 18:0_18:2 ($\beta = -0.232$, FDR-adjusted $q = 3.6 \times 10^{-4}$), and PI 16:0_20:4 ($\beta = -0.228$, FDR-adjusted $q = 0.004$). In contrast, several ether-linked phosphatidylcholines and sphingomyelin species were positively associated with GFATadj, including PC O-16:1/18:1 ($\beta = 0.259$, FDR-adjusted $q = 1.36 \times 10^{-4}$) and SM 34:2; O2 ($\beta = 0.306$, FDR-adjusted $q = 1.16 \times 10^{-4}$) (Supplementary Table S24).

Sensitivity analyses and outlier detection in step-one

Sensitivity analyses using weighted median and MR-Egger methods showed effect directions broadly consistent with the primary IVW estimates, supporting the overall stability of the step-one findings (Supplementary Table S24).

Most lipid outcomes showed no evidence of substantial heterogeneity. However, Cochran's Q tests were significant for 25 traits, with the strongest heterogeneity observed for PI 18:0_18:2 (GCST90277362, MR-Egger Q = 64.802, Q_P = 0.000528; IVW Q = 65.463, Q_P = 0.000648), PI 16:0_18:2 (GCST90277359, MR-Egger Q = 57.602, Q_P = 0.00363; IVW Q = 57.671, Q_P = 0.00497) and PC 18:0_22:6 (GCST90277307, MR-Egger Q = 57.412, Q_P = 0.00381; IVW Q = 57.528, Q_P = 0.00515) (Supplementary Table S25). Consistent with these findings, the MR-PRESSO global test indicated outlier-driven pleiotropy in 19 outcomes, with the strongest signal again observed for PI 18:0_18:2 (RSSobs = 70.867, MRPRESSO_P < 0.001) (Supplementary Table S25).

Directional pleiotropy, as assessed by the MR-Egger intercept, was less common and was observed for only three lipid outcomes: SE 27:1/17:1 (GCST90277243: intercept = 0.02136, SE = 0.00986, P = 0.03780), SE 27:1/18:1 (GCST90277245: intercept = 0.02321, SE = 0.01005, P = 0.02753), and PC 18:0_18:1 (GCST90277299: intercept = 0.02418, SE = 0.01125, P = 0.03923) (Supplementary Table S25).

Integrating evidence from Cochran's Q statistics, MR-Egger intercepts, and MR-PRESSO global tests, 27 lipid outcomes were flagged for further refinement using RadialMR to identify influential outliers before re-analysis (Supplementary Table S25).

Re-analysis Post-RadialMR outlier removal

RadialMR identified and removed 97 outlier SNPs across the 27 flagged lipid outcomes (Supplementary Table S26). After outlier removal, Cochran's Q tests were no longer significant under either the IVW or MR-Egger models, and MR-PRESSO global tests were also non-significant for all re-evaluated outcomes (Supplementary Table S27). MR-Egger intercepts were no longer significant for 25 of the 27 outcomes, with residual marginal pleiotropy remaining only for SE 27:1/18:1 (intercept P = 0.047) and PC 17:0_18:1 (intercept P = 0.017) (Supplementary Table S27).

Post-correction effect directions were broadly consistent with the primary analyses, while statistical support became more selective (Supplementary Table S28). After FDR correction, 16 of the 27 flagged outcomes remained significant, predominantly involving triglycerides, diglycerides, and phosphatidylinositols. Representative strengthened associations included DG 18:1_18:2 (β changed from −0.258 to −0.287; FDR-adjusted $q = 5.63 \times 10^{-5}$), TG 56:4 (β changed from −0.304 to −0.339; FDR-adjusted $q = 1.1 \times 10^{-5}$) and SM d34:2 (FDR-adjusted $q = 7.47 \times 10^{-5}$). By contrast, some borderline associations, including SE 27:1/18:1 and PC 18:0_18:1, became non-significant after outlier removal. For PI 18:0_18:2, inverse estimates were retained in the IVW and weighted

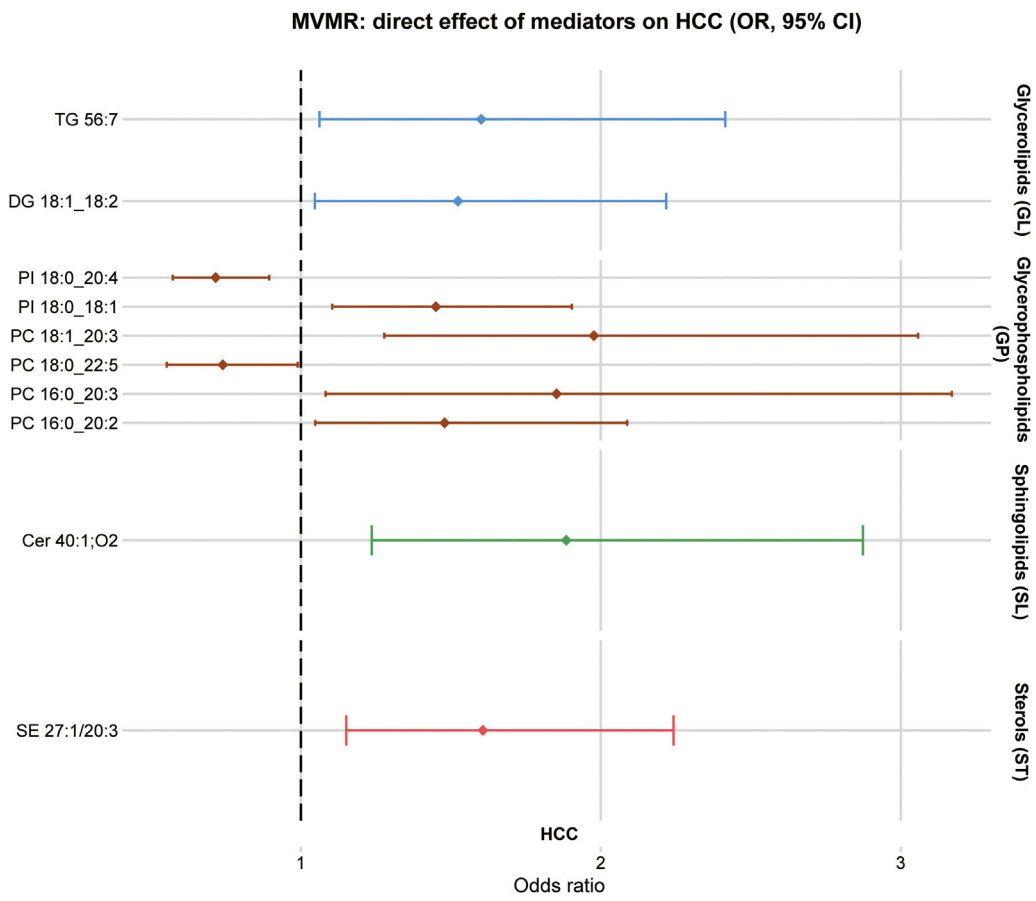


FIGURE 5
Step two MVMR of Two-step Mendelian randomization estimates of the causal associations of each plasma lipid and GFATadj with HCC. Plots (bars) represent OR (95% CI). OR indicates odds ratio.

median analyses, whereas the MR-Egger estimate changed direction (Supplementary Table S28). Visual inspection of funnel, radial, and leave-one-out plots further confirmed the overall stability of the findings (Supplementary Material 2). Based on the prespecified step-one screening and post-correction sensitivity analyses, 91 lipid candidates were carried forward to the second-stage MVMR analyses (Figure 4).

Step-two main results: independent lipid candidates

In the step-two MVMR analyses, 40 lipid candidates were excluded because their conditional F-statistics were below 10, leaving 51 lipids for final analysis (Supplementary Table S22).

After FDR correction, four lipids showed independent associations with HCC in step-two MVMR analyses (Supplementary Table S29). Higher genetically predicted levels of SE 27:1/18:3 (OR = 2.24, 95% CI 1.32–3.80, P = 0.0029, FDR-adjusted q = 0.042), Cer d40:1 (OR = 1.88, 95% CI 1.23–2.87, P = 0.0032, FDR-adjusted q = 0.042), and PC 18:1_20:3 (OR = 1.97, 95% CI 1.28–3.06, P = 0.0022, FDR-adjusted q = 0.042) were associated with higher HCC risk, whereas PI 18:0_20:4 was associated with lower HCC risk (OR = 0.72, 95% CI 0.57–0.89, P = 0.0033, FDR-adjusted q = 0.042).

In addition to these FDR-significant findings, 12 lipids showed nominally significant associations ($P < 0.05$) but did not survive FDR correction (Supplementary Table S29). These included several glycerophospholipids, glycerolipids, sterol esters, and sphingolipid species, such as PI 18:0_18:1, PC 16:0_20:3, TG 56:7, and SE 27:1/20:3. Among them, PC 18:0_22:5 showed a nominal inverse association with HCC (OR = 0.74), with a consistent direction across MVMR-Egger, MVMR-Median, and MVMR-Robust analyses (Supplementary Table S29).

Sensitivity analyses in step-two

Sensitivity analyses in step two were performed using MVMR-Egger, MVMR-Median, and MVMR-Robust methods (Supplementary Table S29). Among the 16 lipids showing FDR-significant or nominally significant associations in the primary MVMR analysis, 10 showed consistent effect directions across all MVMR estimators. These included Cer d40:1, PI 18:0_20:4, and PC 18:1_20:3. By contrast, six lipids showed directional inconsistency across methods; for example, the estimate for SE 27:1/18:3 changed direction in the MVMR-Median and MVMR-Robust analyses.

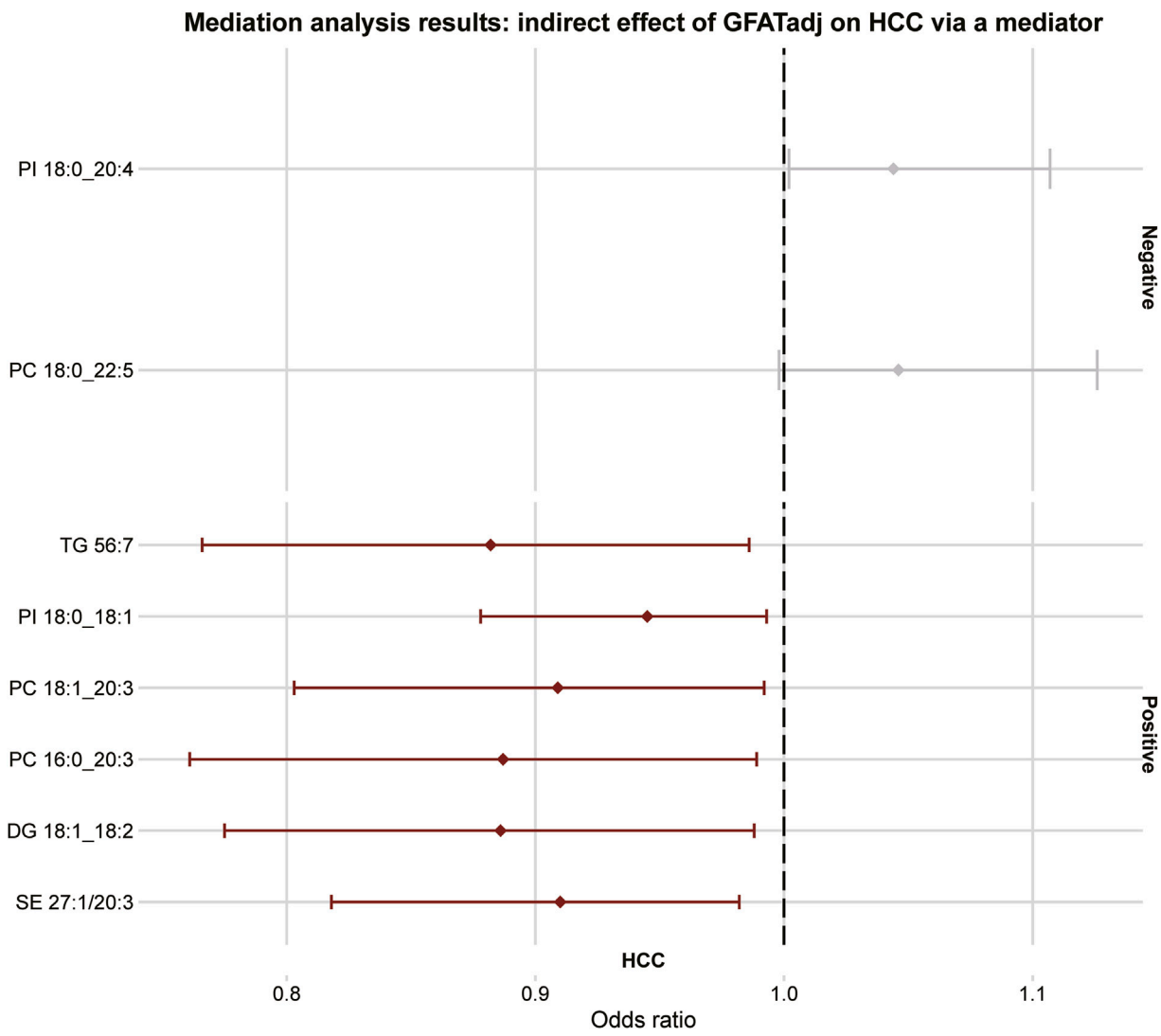


FIGURE 6
Mediation analysis of the association between GFATadj and HCC. Diamonds and horizontal lines represent the estimated indirect effects of the eight plasma lipid mediators, expressed as odds ratios, and their 95% confidence intervals, respectively. Dark red marks significant indirect effects whose direction aligns with the protective total effect of GFATadj on HCC. Grey marks all other indirect effects (non-significant, or significant but opposite in direction). The dashed vertical line denotes the null value (odds ratio = 1).

Cochran's Q test indicated heterogeneity for 13 of the 16 evaluated lipids, whereas PI 18:0_20:4, PI 18:0_18:1, and PC 18:0_22:5 showed no evidence of heterogeneity (Supplementary Table S22). MVMR-Egger intercepts were significant for PC 18:1_20:3, TG 50:4, and TG 54:6, indicating potential directional pleiotropy for these estimates (Supplementary Table S29).

Based on the primary and sensitivity analyses and the prespecified screening criteria, 10 lipids were retained as candidate mediators for reverse MR analysis (Figure 5). These comprised one sterol ester, one ceramide, four phosphatidylcholines, two phosphatidylinositols, one diglyceride, and one triglyceride.

Results of reverse MR analysis

Initial reverse MR analyses across the 10 candidate lipid datasets (9–24 SNPs per dataset, Supplementary Table S30) showed no consistent evidence that the evaluated lipids causally influenced GFATadj. Most estimates were close to the null, although PC 16:0_20:2 showed a nominal association in the weighted median analysis (β = 0.043, P = 0.024) (Supplementary Table S31). Sensitivity analyses identified heterogeneity in five datasets (Cer d40:1, PC 16:0_20:2, PC 18:0_22:5, PC 18:1_20:3, and TG 56:7), with corresponding evidence of outlier-driven distortion in the MR-PRESSO global test (Supplementary Table S32). MR-Egger intercepts were not significant for any dataset.

After RadialMR outlier removal, 2–5 SNPs were excluded from the five flagged datasets, leaving 14–24 instruments per analysis (Supplementary Table S33). Following re-analysis, Cochran's Q tests and MR-PRESSO global tests were no longer significant for any dataset (Supplementary Table S34). Two lipids then showed evidence compatible with reverse causality. PC 16:0_20:2 was positively associated with GFATadj in the IVW analysis (β = 0.038, SE =

0.0135, 95%CI 0.012–0.065, $P = 0.0049$), with a consistent direction in the weighted median and MR-Egger analyses. Cer (d40:1) showed an inverse association with GFATadj in the IVW analysis (β = −0.0380, SE = 0.0177, 95%CI −0.073 to −0.003, $P = 0.0315$), although estimates from the other methods were not statistically significant (Supplementary Table S35).

To minimize potential reverse-causality bias in the mediation framework, PC 16:0_20:2 and Cer d40:1 were excluded from downstream analyses. The remaining eight lipid candidates were retained for formal mediation analysis.

Mediation analysis

Among the eight lipid species entering formal mediation analysis, significant effects were observed for seven, of which six were directionally consistent with the protective total effect (Figure 6; Supplementary Tables S36, S37). For these six species, the estimated mediation proportions ranged from 7.0% to 15.4% (TG 56:7, 15.4%; DG 18:1_18:2, 14.9%; PC 16:0_20:3, 14.8%; SE 27:1/20:3, 11.7%; PC 18:1_20:3, 11.7%; PI 18:0_18:1, 7.0%). PI 18:0_20:4 showed an indirect effect in the direction opposite to the total effect (β = 0.043, SE = 0.026, 95% CI 0.002–0.102; OR = 1.044, 95% CI 1.002–1.107; mediation proportion −5.3%), and therefore does not support a mediating role in the protective association. PC 18:0_22:5, did not show a statistically significant indirect effect, with a confidence interval crossing the null (β = 0.045, SE = 0.032, 95% CI −0.002–0.119; OR = 1.046, 95% CI 0.998–1.126) (Figure 6; Supplementary Table S36).

After correction for multiplicity, seven of the eight indirect effects remained significant, comprising the six species that were directionally consistent with the protective total effect (q = 0.037 in each case) together with PI 18:0_20:4 (q = 0.040); PC 18:0_22:5 was the only species that did not (q = 0.064). The indirect effect, 95% confidence interval, OR, P value and FDR-adjusted q value for each of the eight species are reported in Supplementary Table S36.

From the shared SNP-level data, the sampling correlation between the two component estimates ranged from ρ = −0.057 to +0.015 across the eight lipid species entering mediation analysis. Retaining the covariance term changed the standard error of the indirect effect by at most 2.5% in absolute terms (Supplementary Table S39) and did not affect the significance of any indirect effect, defined as a 95% confidence interval excluding the null. When ρ was varied from −0.50 to +0.50 in steps of 0.01 using the same distribution-of-the-product method, the set of significant indirect effects was unchanged (Supplementary Table S39).

Colocalization analysis of prioritized lipid–HCC loci

Bayesian colocalization was performed for every independent genome-wide significant locus of the lipid species showing directionally consistent indirect effects (28 loci across six species; Table 2; Supplementary Table S38), to assess whether the observed associations were consistent with shared causal variants. Colocalization was not supported at any locus. At the primary locus of SE 27:1/20:3 the regional signal was specific to the lipid (rs1135999; PP.H1 = 0.895, PP.H4 = 0.031). PI 18:0_18:1 showed the strongest colocalization signal of the six species, but PP.H4 remained below the prespecified threshold of 0.80 (rs641738; PP.H4 = 0.597, PP.H3 = 0.076). At the primary loci of the remaining mediators, PP.H4 ranged from 0.031 to 0.163 (TG 56:7, rs174554; DG 18:1_18:2, rs964184; and PC 16:0_20:3 and PC 18:1_20:3, which share the lead SNP rs6498540). Across all 28 loci, PP.H4 exceeded 0.35 only at the PI 18:0_18:1 locus described above and at a second independent locus of PC 18:1_20:3 (rs150057262; PP.H4 = 0.612, PP.H3 = 0.388), 0.612 being the highest value observed. Conversely, two loci provided positive evidence for distinct rather than shared causal variants (SE 27:1/20:3, rs187429064, PP.H3 = 0.952; TG 56:7, rs182611493, PP.H3 = 0.669). Overall, the colocalization analyses did not provide consistent strong support for shared causal variants; complete results for all 28 loci are provided in Supplementary Table S38.

Discussion

In this Mendelian randomization study, genetically predicted GFATadj was inversely associated with HCC risk, and this association remained after adjustment for other fat-depot phenotypes and related metabolic and behavioral risk factors. By contrast, no significant associations were observed for VATadj or ASATadj, although these null findings should be interpreted cautiously given the limited statistical power for these traits. Beyond the primary association analyses, two-step MR identified seven lipid species with a significant indirect effect, six of which were directionally consistent with the protective total effect and are therefore interpreted as candidate partial mediators of the association between GFATadj and HCC: TG 56:7 (15.4%), DG 18:1_18:2 (14.9%), PC 16:0_20:3 (14.8%), SE 27:1/20:3 (11.7%), PC 18:1_20:3 (11.7%) and PI 18:0_18:1 (7.0%). One further species, PI 18:0_20:4, showed a significant indirect effect in the opposite direction and is not interpreted as a mediator of the protective association. Taken together, these findings support a potentially protective role of gluteofemoral fat distribution in HCC and point to specific lipid pathways that may contribute to this relationship.

Our findings are broadly consistent with prior imaging-based studies suggesting that lower-body adiposity may be metabolically protective, whereas visceral adiposity may not show the same relationship. In particular, Gupta et al. reported that higher lower-body subcutaneous fat was associated with reduced cancer incidence, whereas visceral adipose tissue was not significantly associated with cancer risk in multivariable models [58]. The present study extends those observations in several ways. First, we focused specifically on HCC rather than heterogeneous cancer outcomes. Second, we used MRI-derived, body-size-independent depot phenotypes, which better isolate regional adiposity from overall body size. Third, by applying an MR framework, we provide genetically informed evidence supporting an inverse association between gluteofemoral fat distribution and HCC risk.

In contrast to imaging-based studies, several observational studies using anthropometric measures have suggested a different risk pattern. For example, Florio et al. reported positive associations between waist circumference and primary liver cancer risk, and meta-analytic evidence has further linked both waist and hip circumference to higher liver cancer risk [13, 59]. Similarly, several studies have suggested that visceral fat accumulation is associated with increased liver cancer risk [15, 60, 61].

TABLE 2 Bayesian colocalization results for prioritized lipid–HCC loci.

Lipid	Overlapping SNPs	PP.H1	PP.H3	PP.H4	Interpretation
SE 27:1/20:3	915	0.895	0.074	0.031	Lipid-specific signal; no colocalization support
DG 18:1_18:2	2333	0.788	0.167	0.046	Lipid-specific signal; no colocalization support
PC 16:0_20:3	909	0.896	0.073	0.031	Lipid-specific signal; no colocalization support
PC 18:1_20:3	910	0.896	0.073	0.031	Lipid-specific signal; no colocalization support
PI 18:0_18:1	2383	0.327	0.076	0.597	Suggestive colocalization
TG 56:7	1652	0.728	0.109	0.163	Lipid-specific signal; no colocalization support

These findings are not necessarily incompatible with our results, but they likely reflect important differences in phenotyping. Anthropometric indices such as waist and hip circumference are composite measures that do not isolate specific adipose depots and may reflect varying contributions from visceral fat, abdominal subcutaneous fat, gluteofemoral fat, and lean mass [62, 63]. Consistent with this, in the Liver Cancer Pooling Project the association of hip circumference with liver cancer was entirely accounted for by waist circumference [59]. In particular, a higher waist-to-hip ratio may arise from greater visceral or abdominal adiposity, lower gluteofemoral fat, or both. These conventional measures are often insufficiently adjusted for overall body size, and residual correlations with height or general adiposity may obscure depot-specific effects [11]. By contrast, MRI provides a more anatomically specific assessment of regional and ectopic fat distribution than anthropometric proxies such as waist and hip circumference [64]. Therefore, the MRI-derived VATadj and GFATadj phenotypes used in our study may better isolate depot-specific adiposity independent of overall body size, which may partly explain why our findings differ from those based on anthropometric measures.

A plausible biological explanation for the inverse association between GFATadj and HCC risk lies in differences in lipid handling and ectopic fat buffering. Lipid metabolic dysregulation has been increasingly implicated in hepatocarcinogenesis [65]. In contrast to visceral adipose tissue, gluteofemoral fat has been proposed to function as a relatively protective metabolic sink, sequestering circulating fatty acids and thereby limiting their ectopic deposition in the liver [66]. By buffering excess lipid flux, greater gluteofemoral fat capacity may reduce hepatic lipotoxic stress and insulin resistance. This mechanism is consistent with the hypothesis that the association between GFATadj and HCC may be mediated, at least in part, through alterations in circulating lipid profiles.

Previous studies have described a characteristic lipidomic profile associated with general obesity, including higher levels of several cholesteryl ester, diglyceride, triglyceride, and sphingomyelin species [67, 68]. In contrast, our MR analyses suggest that GFATadj is associated with a distinct, and in several respects directionally opposite, lipidomic pattern. In particular, greater GFATadj was associated with lower levels of multiple triglyceride and diglyceride species, consistent with a more favorable lipid-storage profile. This contrast is illustrated by TG 56:4 and TG 56:5, which have been reported to increase with BMI [69], whereas in our analyses higher GFATadj was associated with lower levels of these species. Taken together, these findings support the idea that gluteofemoral fat distribution may buffer against the dyslipidemic milieu typically linked to general obesity, providing a plausible metabolic context for its inverse association with HCC risk.

Among the species screened, six showed indirect effects in the direction of the protective total effect. Prior lipidomic studies have reported elevated levels of PI 18:0_18:1 in patients with HCC [21], and our MVMR and mediation analyses were directionally consistent with a role for this lipid as a candidate partial mediator linking GFATadj to HCC. At the same time, not all lipids reported to differ in observational HCC studies appeared to function as mediators in our MR framework. Specifically, Lee et al. reported differential abundance of LPC (18:2), PI (16:0_20:4), and PI (18:0_20:3) in HCC patients [21], whereas Cotte et al. observed altered LPC (20:4) in those with cirrhosis [70]. Nevertheless, our analyses did not support a comparable mediator role, and reverse-direction analyses suggested that some of these alterations may instead reflect downstream consequences of disease liability. This distinction is important, because lipids associated with established HCC may still serve as disease-related biomarkers, even if they do not represent causal mediators or therapeutic targets.

Our results also highlight specific lipid species that may be relevant to HCC risk. The first two of the six lipid species were glycerolipids, TG 56:7 and DG 18:1_18:2, for which the estimated mediated proportions were the two largest observed (15.4% and 14.9%). Direct species-level evidence for either lipid in liver disease is not available, but two lines of evidence are relevant. First, hepatic glycerolipid metabolism occupies a central position in the pathways linking adipose distribution to liver disease [71]: diacylglycerols circulate in part as hepatic secretory products, and a selective postprandial rise in hepatic-derived diacylglycerol species is an early feature of MAFLD that correlates with postprandial insulin concentrations [72]. Within the liver, cytosolic diacylglycerol activates protein kinase Cε and impairs insulin signaling [73], a mechanism relevant because insulin resistance is an established contributor to hepatocarcinogenesis [65]. Independently of insulin signaling, membrane diacylglycerol and ceramide sustain Wnt/β-catenin signaling and promote HCC cell proliferation, tumor growth, and migration [74]. Hepatic diacylglycerol disposal also appears relevant: DGAT2, which channels diacylglycerol toward triglyceride synthesis, is downregulated in human HCC tissue and its overexpression suppresses HCC cell proliferation and tumor growth [75], and lipidomic profiling of MAFLD-associated HCC identified di- and triglyceride species among its most differentially abundant lipids [76]. Second, an independent MR study using the

same 179-species lipid GWAS reported two other 56-carbon triglycerides, TG 56:3 and TG 56:4, as associated with lower hepatic cancer risk [77], although it did not report TG 56:7 and its Steiger test did not support a unidirectional effect for either species; the same study found DG 18:1_18:2 protective against breast cancer, with directionality supported. These observations, although indirect, are compatible with a contribution of these glycerolipids to HCC risk through hepatic glycerolipid handling.

The next two were diacyl phosphatidylcholines: PC 16:0_20:3 (mediated proportion 14.8%) and PC 18:1_20:3 (11.7%). The latter was the only one of the six directionally consistent mediators to show a step-two association with HCC that survived FDR correction (OR = 1.98, 95% CI 1.28–3.06, P = 0.0022, q = 0.042). Both carry a 20:3 acyl chain, consistent with dihomo-γ-linolenic acid (20:3 n-6), pointing to phosphatidylcholine remodeling and n-6 fatty-acid handling as a further, partially distinct route. Human HCC tissue shows increased LPCAT1, the enzyme that converts lysophosphatidylcholine into phosphatidylcholine during Lands-cycle remodeling, together with enrichment of phosphatidylcholine species carrying palmitoleic or oleic acid at the sn-2 position; LPCAT1 overexpression promoted proliferation, migration, and invasion in HCC cell lines [78]. The 20:3 (n-6) chain lies at a branch point between anti-inflammatory derivatives and, through arachidonic acid, pro-inflammatory lipid mediators, and its abundance is governed largely by Δ6-and Δ5-desaturase activity [79, 80]. Higher serum dihomo-γ-linolenic acid and lower estimated Δ5-desaturase activity have been associated with hepatic steatosis in addition to conventional metabolic syndrome components [81], and Mendelian randomization has linked genetically proxied PUFA desaturase activity, with dihomo-γ-linolenic acid among the potential mediators, to the risk of several cancers [82]. Stearoyl-CoA desaturase 1, which generates the Δ9-monounsaturated 18:1 chain, is also overexpressed in HCC and has been linked to proliferation, chemoresistance, invasion, and metastasis [83, 84].

Beyond the lipid species already discussed, SE 27:1/20:3 was identified as having a significant indirect effect, suggesting that cholesterol ester metabolism may be one pathway linking favorable adipose distribution to lower HCC risk. This pathway has been implicated in liver cancer progression [85]. In HCC, upregulation of sterol O-acyltransferases 1 (SOAT1) promotes the conversion of free cholesterol into cholesteryl esters that are stored in lipid droplets, contributing to metabolic adaptations that support tumor growth [86]. Within this context, the inverse association between GFATadj and SE 27:1/20:3 is compatible with the idea that gluteofemoral fat may act as a relatively protective metabolic sink, reducing circulating lipid overflow and limiting substrate availability for hepatic cholesterol esterification [87, 88].

In addition to the cholesterol ester-related findings, PI 18:0_18:1 was another lipid with a significant indirect effect. However, its effect was the small (β = −0.057) and its upper confidence limit lay close to zero (−0.007). Therefore, it is best interpreted as a suggestive mediator. Phosphatidylinositol species are precursors for phosphoinositides, which are central to membrane-associated signaling processes and have been implicated in oncogenic pathway regulation [89–91]. Prior studies have reported enrichment of PI 18:0_18:1 or closely related phosphatidylinositol species in malignant tissues [92, 93], and our findings are directionally consistent with the possibility that this lipid contributes to the metabolic signaling context linking adipose distribution to HCC risk.

Bayesian colocalization provided only limited locus-level support for shared causal variants. PP.H4 at 28 loci never approached the prespecified threshold of 0.80, whereas PP.H1 exceeded 0.5 at 24 loci and the HCC-side regional association did not reach genome-wide significance at 25 loci. The analysis was limited less by evidence against sharing than by a weak outcome-side signal: with 500 HCC cases, a lipid-dominant posterior is expected even when both traits share a causal variant. Where the HCC signal was strong the posteriors were more discriminating: in the 19p13.11 (TM6SF2–NCAN) region a shared causal variant was favored for PC 18:1_20:3 (PP.H4 = 0.612), whereas distinct causal variants were favored for SE 27:1/20:3 (PP.H3 = 0.952) and TG 56:7 (PP.H3 = 0.669). Mediator loci mapped predominantly to genes governing lipid handling and liver disease, including FADS1/FADS2, which synthesize the 20:3 n-6 chains of both phosphatidylcholine mediators, and MBOAT7, TM6SF2–NCAN, APOA5–APOC3–BUD13, APOE, GCKR, LPL and HNF4A. The locus-level evidence does not establish mediation, and these pathways remain candidate mechanisms requiring validation in larger HCC datasets and conditional colocalization approaches [94].

Several limitations of our study warrant discussion. While the Mendelian randomization framework strengthens causal inference compared to observational designs, it does not elucidate precise molecular mechanisms. This is particularly relevant for the following six lipid species: TG 56:7, PI 18:0_18:1, PC 18:1_20:3, PC 16:0_20:3, DG 18:1_18:2, and SE 27:1/20:3, for which direct functional evidence in HCC remains limited. Existing mechanistic studies have focused largely on broader lipid classes rather than on individual molecular species, making it difficult to determine whether these lipids act as active effectors or instead reflect downstream correlates of the protective influence of gluteofemoral fat. Accordingly, these findings should be interpreted as highlighting hypothesis-generating candidate mediators that require further experimental validation or prospective or population-based clinical validation.

Additional limitations should also be acknowledged. First, the number of HCC cases in the discovery dataset was modest, which limited statistical power for some analyses, particularly those involving VATadj and ASATadj. Second, the replication analysis used primary liver cancer rather than strictly defined HCC as the outcome, which may have introduced some phenotypic heterogeneity. Third, all analyses were restricted to individuals of European ancestry, and the generalizability of these findings to other populations remains uncertain. Finally, the sex-stratified analyses were exploratory and were based on a small number of instruments together with a non-sex-specific outcome; they therefore cannot establish a sex-specific effect on HCC. The apparent numerical difference between the male- and female-specific estimates may reflect differences in instrument number and strength, differential statistical power, or chance variation rather than a true biological difference.

Conclusion

This study suggests that MRI-derived gluteofemoral adiposity adjusted for BMI and height (GFATadj) is inversely associated with HCC risk in an MR framework. Among the evaluated lipid candidates, six species may represent candidate partial mediators of this association. These findings support the relevance of depot-specific adiposity and lipid metabolic pathways in HCC, while further functional and population-based validation is needed to clarify the underlying mechanisms.

Author contributions

HL and JY conceptualized and designed the study. HL, FW, RL, and JY contributed to the design of methodology. HL, RL, and JT conducted the data collection and organization work. HL, FW, and RL made substantial contributions to data cleaning, analysis, and interpretation. HL wrote the first version of the manuscript. XJ and JZ contributed to revise the manuscript for grammar and writing style. XJ and JY were responsible for revising the manuscript. All authors contributed to the article and approved the submitted version.

Data availability

The original contributions presented in the study are included in the article/Supplementary Material, further inquiries can be directed to the corresponding author.

Ethics statement

Ethical approval was not required for the study involving humans in accordance with the local legislation and institutional requirements. Written informed consent to participate in this study was not required from the participants or the participants' legal guardians/next of kin in accordance with the national legislation and the institutional requirements.

Funding

The author(s) declared that financial support was not received for this work and/or its publication.

Acknowledgments

We thank the participants and investigators of the FinnGen study, the Million Veterans Program, and GeneRISK cohort. We also thank Marina Vabistsevits, Aida Seyedsalehi and their respective research teams for their invaluable contributions. Their code, made available on GitHub (https://github.com/mvab/mendelian-randomization-breast-cancer, and https://github.com/as2970/EA_brain_AD_MR), significantly facilitated our analyses.

Conflict of interest

The author(s) declared no potential conflicts of interest with respect to the research, authorship, and/or publication of this article.

Generative AI statement

The author(s) declared that generative AI was used in the creation of this manuscript. During the preparation of this work, the authors used a generative AI tool as follows: DeepSeek (DeepSeek AI; model deepseek-v4-flash; accessed through the DeepSeek API, https://api.deepseek.com) was used to edit the manuscript text for grammar, clarity, and consistency of terminology, and to assist with auditing the analysis scripts. Generative AI was not used to generate, alter, or fabricate data, results, or figures; all figures were generated from the authors' analysis code and were not produced or edited by AI. No AI tool is listed as an author. All AI-assisted output was reviewed, validated, and corrected by the authors, and the authors take full responsibility for the accuracy, originality, and integrity of the content of this publication.

Any alternative text (alt text) provided alongside figures in this article has been generated by Frontiers with the support of artificial intelligence and reasonable efforts have been made to ensure accuracy, including review by the authors wherever possible. If you identify any issues, please contact us.

Supplementary material

The Supplementary Material for this article can be found online at: https://www.ebm-journal.org/articles/10.3389/ebm.2026.11173/full#supplementary-material

References

1. Sung H, Ferlay J, Siegel RL, Laversanne M, Soerjomataram I, Jemal A, et al. Global cancer statistics 2020: GLOBOCAN estimates of incidence and mortality worldwide for 36 cancers in 185 countries. *CA Cancer J Clin* (2021) 71(3):209–49. doi: 10.3322/caac.21660

2. McGlynn KA, Petrick JL, El-Serag HB. Epidemiology of hepatocellular carcinoma. *Hepatology* (2021) 73(Suppl. 1):4–13. doi: 10.1002/hep.31288

3. Singal AG, Kanwal F, Llovet JM. Global trends in hepatocellular carcinoma epidemiology: implications for screening, prevention and therapy. *Nat Rev Clin Oncol* (2023) 20(12):864–84. doi: 10.1038/s41571-023-00825-3

4. Liu J, Ayada I, Zhang X, Wang L, Li Y, Wen T, et al. Estimating global prevalence of metabolic dysfunction-associated fatty liver disease in overweight or Obese adults. *Clin Gastroenterol Hepatol* (2022) 20(3):e573–e582. doi: 10.1016/j.cgh.2021.02.030

5. Gan L, Liu Z, Sun C. Obesity linking to hepatocellular carcinoma: a global view. *Biochim Biophys Acta Rev Cancer* (2018) 1869(2):97–102. doi: 10.1016/j.bbcan.2017.12.006

6. Rajesh Y, Sarkar D. Molecular mechanisms regulating obesity-associated hepatocellular carcinoma. *Cancers (Basel)* (2020) 12(5):1290. doi: 10.3390/cancers12051290

7. Lauby-Secretan B, Scoccianti C, Loomis D, Grosse Y, Bianchini F, Straif K, et al. Body fatness and cancer-viewpoint of the IARC working group. *N Engl J Med* (2016) 375(8):794–8. doi: 10.1056/NEJMsr1606602

8. Renehan AG, Tyson M, Egger M, Heller RF, Zwahlen M. Body-mass index and incidence of cancer: a systematic review and meta-analysis of prospective observational studies. *Lancet* (2008) 371(9612):569–78. doi: 10.1016/S0140-6736(08)60269-X

9. Vithayathil M, Carter P, Kar S, Mason AM, Burgess S, Larsson SC. Body size and composition and risk of site-specific cancers in the UK Biobank and large international consortia: a mendelian randomisation study. *Plos Med* (2021) 18(7):e1003706. doi: 10.1371/journal.pmed.1003706

10. Karpe F, Pinnick KE. Biology of upper-body and lower-body adipose tissue-link to whole-body phenotypes. *Nat Rev Endocrinol* (2015) 11(2):90–100. doi: 10.1038/nrendo.2014.185

11. Agrawal S, Wang M, Klarqvist M, Smith K, Shin J, Dashti H, et al. Inherited basis of visceral, abdominal subcutaneous and gluteofemoral fat depots. *Nat Commun* (2022) 13(1):3771. doi: 10.1038/s41467-022-30931-2

12. Pulit SL, Stoneman C, Morris AP, Wood AR, Glastonbury CA, Tyrrell J, et al. Meta-analysis of genome-wide association studies for body fat distribution in 694 649 individuals of European ancestry. *Hum Mol Genet* (2019) 28(1):166–74. doi: 10.1093/hmg/ddy327

13. Yan LJ, Yang LS, Yan YC, Tan SY, Ding ZN, Liu H, et al. Anthropometric indicators of adiposity and risk of primary liver cancer: a systematic review and dose-response meta-analysis. *Eur J Cancer* (2023) 185:150–63. doi: 10.1016/j.ejca.2023.03.005

14. Vongsuvanh R, George J, Qiao L, van der Poorten D. Visceral adiposity in gastrointestinal and hepatic carcinogenesis. *Cancer Lett* (2013) 330(1):1–10. doi: 10.1016/j.canlet.2012.11.038

15. Xu FQ, Xu QY, Zhu ZJ, Jin L, Ye TW, Du CF, et al. Visceral and ectopic fat are more predictively associated with primary liver cancer than overall obesity from genetic sights: a Mendelian randomization study. *Int J Cancer* (2024) 154(3):530–7. doi: 10.1002/ijc.34751

16. Fox CS, Liu Y, White CC, Feitosa M, Smith AV, Heard-Costa N, et al. Genome-wide association for abdominal subcutaneous and visceral adipose reveals a novel locus for visceral fat in women. *Plos Genet* (2012) 8(5):e1002695. doi: 10.1371/journal.pgen.1002695

17. Pietiläinen KH, Kaye S, Karmi A, Suojanen L, Rissanen A, Virtanen KA. Agreement of bioelectrical impedance with dual-energy X-ray absorptiometry and MRI to estimate changes in body fat, skeletal muscle and visceral fat during a 12-month weight loss intervention. *Br J Nutr* (2013) 109(10):1910–6. doi: 10.1017/S0007114512003698

18. Gagnon E, Paulin A, Mitchell PL, Arsenault BJ. Disentangling the impact of gluteofemoral *versus* visceral fat accumulation on cardiometabolic health using sex-stratified Mendelian randomization. *Atherosclerosis* (2023) 386:117371. doi: 10.1016/j.atherosclerosis.2023.117371

19. Quehenberger O, Dennis EA. The human plasma lipidome. *N Engl J Med* (2011) 365(19):1812–23. doi: 10.1056/NEJMra1104901

20. Hornburg D, Wu S, Moqri M, Zhou X, Contrepois K, Bararpour N, et al. Dynamic lipidome alterations associated with human health, disease and ageing. *Nat Metab* (2023) 5(9):1578–94. doi: 10.1038/s42255-023-00880-1

21. Lee GB, Lee JC, Moon MH. Plasma lipid profile comparison of five different cancers by nanoflow ultrahigh performance liquid chromatography-tandem mass spectrometry. *Anal Chim Acta* (2019) 1063:117–26. doi: 10.1016/j.aca.2019.02.021

22. Zhang Q, Tong M, Xu H, Yin Y, Gao P, Bi K, et al. Accurate determination for lipidomics based on LC-tandem-MS parameters modeling, prediction, and database: monitoring the progression of hepatocellular carcinoma. *J Pharm Biomed Anal* (2023) 223:115126. doi: 10.1016/j.jpba.2022.115126

23. Relton CL, Davey Smith G. Two-step epigenetic Mendelian randomization: a strategy for establishing the causal role of epigenetic processes in pathways to disease. *Int J Epidemiol* (2012) 41(1):161–76. doi: 10.1093/ije/dyr233

24. Vabistsevits M, Davey Smith G, Sanderson E, Richardson TG, Lloyd-Lewis B, Richmond RC. Deciphering how early life adiposity influences breast cancer risk using Mendelian randomization. *Commun Biol* (2022) 5(1):337. doi: 10.1038/s42003-022-03272-5

25. Skrivankova VW, Richmond RC, Woolf BAR, Yarmolinsky J, Davies NM, Swanson SA, et al. Strengthening the reporting of observational studies in epidemiology using mendelian randomization: the STROBE-MR statement. *JAMA* (2021) 326(16):1614–21. doi: 10.1001/jama.2021.18236

26. Kurki MI, Karjalainen J, Palta P, Sipilä TP, Kristiansson K, Donner KM, et al. FinnGen provides genetic insights from a well-phenotyped isolated population. *Nature* (2023) 613(7944):508–18. doi: 10.1038/s41586-022-05473-8

27. Gaziano JM, Concato J, Brophy M, Fiore L, Pyarajan S, Breeling J, et al. Million veteran program: a mega-biobank to study genetic influences on health and disease. *J Clin Epidemiol* (2016) 70:214–23. doi: 10.1016/j.jclinepi.2015.09.016

28. Verma A, Huffman JE, Rodriguez A, Conery M, Liu M, Ho YL, et al. Diversity and scale: genetic architecture of 2068 traits in the VA million veteran program. *Science* (2024) 385(6706):eadj1182. doi: 10.1126/science.adj1182

29. Ottensmann L, Tabassum R, Ruotsalainen SE, Gerl MJ, Klose C, Widén E, et al. Genome-wide association analysis of plasma lipidome identifies 495 genetic associations. *Nat Commun* (2023) 14(1):6934. doi: 10.1038/s41467-023-42532-8

30. Liu M, Jiang Y, Wedow R, Li Y, Brazel DM, Chen F, et al. Association studies of up to 1.2 million individuals yield new insights into the genetic etiology of tobacco and alcohol use. *Nat Genet* (2019) 51(2):237–44. doi: 10.1038/s41588-018-0307-5

31. Vogelezang S, Bradfield JP, Ahluwalia TS, Curtin JA, Lakka TA, Grarup N, et al. Novel loci for childhood body mass index and shared heritability with adult cardiometabolic traits. *Plos Genet* (2020) 16(10):e1008718. doi: 10.1371/journal.pgen.1008718

32. Xue A, Wu Y, Zhu Z, Zhang F, Kemper KE, Zheng Z, et al. Genome-wide association analyses identify 143 risk variants and putative regulatory mechanisms for type 2 diabetes. *Nat Commun* (2018) 9(1):2941. doi: 10.1038/s41467-018-04951-w

33. 1000 Genomes Project Consortium, Auton A, Brooks LD, Durbin RM, Garrison EP, Kang HM, et al. A global reference for human genetic variation. *Nature* (2015) 526(7571):68–74. doi: 10.1038/nature15393

34. Yeung C, Schooling CM. Systemic inflammatory regulators and risk of Alzheimer's disease: a bidirectional Mendelian-randomization study. *Int J Epidemiol* (2021) 50(3):829–40. doi: 10.1093/ije/dyaa241

35. Xiang M, Wang Y, Gao Z, Wang J, Chen Q, Sun Z, et al. Exploring causal correlations between inflammatory cytokines and systemic lupus erythematosus: a Mendelian randomization. *Front Immunol* (2022) 13:985729. doi: 10.3389/fimmu.2022.985729

36. Burgess S, Thompson SG. CRP CHD genetics collaboration. Avoiding bias from weak instruments in Mendelian randomization studies. *Int J Epidemiol* (2011) 40(3):755–64. doi: 10.1093/ije/dyr036

37. Shim H, Chasman DI, Smith JD, Mora S, Ridker PM, Nickerson DA, et al. A multivariate genome-wide association analysis of 10 LDL subfractions, and their response to statin treatment, in 1868 Caucasians. *PLoS One* (2015) 10(4):e0120758. doi: 10.1371/journal.pone.0120758

38. Sanderson E, Spiller W, Bowden J. Testing and correcting for weak and pleiotropic instruments in two-sample multivariable Mendelian randomization. *Stat Med* (2021) 40(25):5434–52. doi: 10.1002/sim.9133

39. Sanderson E, Davey Smith G, Windmeijer F, Bowden J. An examination of multivariable Mendelian randomization in the single-sample and two-sample summary data settings. *Int J Epidemiol* (2019) 48(3):713–27. doi: 10.1093/ije/dyy262

40. Burgess S. Sample size and power calculations in Mendelian randomization with a single instrumental variable and a binary outcome. *Int J Epidemiol* (2014) 43(3):922–9. doi: 10.1093/ije/dyu005

41. Burgess S, Butterworth A, Thompson SG. Mendelian randomization analysis with multiple genetic variants using summarized data. *Genet Epidemiol* (2013) 37(7):658–65. doi: 10.1002/gepi.21758

42. Bowden J, Davey Smith G, Burgess S. Mendelian randomization with invalid instruments: effect estimation and bias detection through Egger regression. *Int J Epidemiol* (2015) 44(2):512–25. doi: 10.1093/ije/dyv080

43. Bowden J, Davey Smith G, Haycock PC, Burgess S. Consistent estimation in Mendelian randomization with some invalid instruments using a weighted median estimator. *Genet Epidemiol* (2016) 40(4):304–14. doi: 10.1002/gepi.21965

44. Davies NM, Holmes MV, Davey Smith G. Reading Mendelian randomisation studies: a guide, glossary, and checklist for clinicians. *BMJ* (2018) 362:k601. doi: 10.1136/bmj.k601

45. Burgess S, Bowden J, Fall T, Ingelsson E, Thompson SG. Sensitivity analyses for robust causal inference from mendelian randomization analyses with multiple genetic variants. *Epidemiology* (2017) 28(1):30–42. doi: 10.1097/EDE.0000000000000559

46. Verbanck M, Chen C, Neale B, Do R. Detection of widespread horizontal pleiotropy in causal relationships inferred from Mendelian randomization between complex traits and diseases. *Nat Genet* (2018) 50(5):693–8. doi: 10.1038/s41588-018-0099-7

47. Bowden J, Spiller W, Fabiola Del Greco M, Sheehan N, Thompson J, Minelli C, et al. Improving the visualization, interpretation and analysis of two-sample summary data Mendelian randomization *via* the radial plot and radial regression. *Int J Epidemiol* (2018) 47(4):1264–78. doi: 10.1093/ije/dyy101

48. Zheng J, Baird D, Borges MC, Bowden J, Hemani G, Haycock P, et al. Recent developments in Mendelian randomization studies. *Curr Epidemiol Rep* (2017) 4(4):330–45. doi: 10.1007/s40471-017-0128-6

49. Carter AR, Sanderson E, Hammerton G, Richmond RC, Davey Smith G, Heron J, et al. Mendelian randomisation for mediation analysis: current methods and challenges for implementation. *Eur J Epidemiol* (2021) 36(5):465–78. doi: 10.1007/s10654-021-00757-1

50. Burgess S, Thompson SG. Multivariable Mendelian randomization: the use of pleiotropic genetic variants to estimate causal effects. *Am J Epidemiol* (2015) 181(4):251–60. doi: 10.1093/aje/kwu283

51. Tofighi D, MacKinnon DP. RMediation: an R package for mediation analysis confidence intervals. *Behav Res Methods* (2011) 43(3):692–700. doi: 10.3758/s13428-011-0076-x

52. MacKinnon DP, Fritz MS, Williams J, Lockwood CM. Distribution of the product confidence limits for the indirect effect: program PRODCLIN. *Behav Res Methods* (2007) 39(3):384–9. doi: 10.3758/bf03193007

53. Meeker WQ, Escobar LA. An algorithm to compute the cdf of the product of two normal random variables. *Commun Stat Simul Comput* (1994) 23(1):271–80. doi: 10.1080/03610919408813168

54. Craig CC. On the frequency function of xy. *Ann Math Stat* (1936) 7:1–15. doi: 10.1214/aoms/1177732541

55. Grant AJ, Burgess S. Pleiotropy robust methods for multivariable Mendelian randomization. *Stat Med* (2021) 40(26):5813–30. doi: 10.1002/sim.9156

56. Giambartolomei C, Vukcevic D, Schadt EE, Franke L, Hingorani AD, Wallace C, et al. Bayesian test for colocalisation between pairs of genetic association studies using summary statistics. *Plos Genet* (2014) 10(5):e1004383. doi: 10.1371/journal.pgen.1004383

57. Benjamini Y, Hochberg Y. Controlling the false discovery rate: a practical and powerful approach to multiple testing. *J R Stat Soc Ser B Stat Methodol* (1995) 57(1):289–300. doi: 10.1111/j.2517-6161.1995.tb02031.x

58. Gupta A, Pandey A, Ayers C, Beg MS, Lakoski SG, Vega GL, et al. An analysis of individual body fat depots and risk of developing cancer: insights from the Dallas heart study. *Mayo Clin Proc* (2017) 92(4):536–43. doi: 10.1016/j.mayocp.2016.12.023

59. Florio AA, Campbell PT, Zhang X, Zeleniuch-Jacquotte A, Wactawski-Wende J, Smith-Warner SA, et al. Abdominal and gluteofemoral size and risk of liver cancer: the liver cancer pooling project. *Int J Cancer* (2020) 147(3):675–85. doi: 10.1002/ijc.32760

60. Montano-Loza AJ, Mazurak VC, Ebadi M, Meza-Junco J, Sawyer MB, Baracos VE, et al. Visceral adiposity increases risk for hepatocellular carcinoma in male patients with cirrhosis and recurrence after liver transplant. *Hepatology* (2018) 67(3):914–23. doi: 10.1002/hep.29578

61. Imai K, Takai K, Miwa T, Maeda T, Hanai T, Shirakami Y, et al. Higher accumulation of visceral adipose tissue is an independent risk factor for hepatocellular carcinoma among viral hepatitis patients with non-cirrhotic livers. *Cancers (Basel)* (2021) 13(23):5980. doi: 10.3390/cancers13235980

62. Iacobellis G. Imaging of visceral adipose tissue: an emerging diagnostic tool and therapeutic target. *Curr Drug Targets Cardiovasc Haematol Disord* (2005) 5(4):345–53. doi: 10.2174/1568006054553408

63. Graffy PM, Pickhardt PJ. Quantification of hepatic and visceral fat by CT and MR imaging: relevance to the obesity epidemic, metabolic syndrome and NAFLD. *Br J Radiol* (2016) 89(1062):20151024. doi: 10.1259/bjr.20151024

64. Neeland IJ, Ross R, Després JP, Matsuzawa Y, Yamashita S, Shai I, et al. Visceral and ectopic fat, atherosclerosis, and cardiometabolic disease: a position statement. *Lancet Diabetes Endocrinol* (2019) 7(9):715–25. doi: 10.1016/S2213-8587(19)30084-1

65. Du D, Liu C, Qin M, Zhang X, Xi T, Yuan S, et al. Metabolic dysregulation and emerging therapeutical targets for hepatocellular carcinoma. *Acta Pharm Sin B* (2022) 12(2):558–80. doi: 10.1016/j.apsb.2021.09.019

66. Alser M, Naja K, Elrayess MA. Mechanisms of body fat distribution and gluteal-femoral fat protection against metabolic disorders. *Front Nutr* (2024) 11:1368966. doi: 10.3389/fnut.2024.1368966

67. Yin X, Willinger CM, Keefe J, Liu J, Fernández-Ortiz A, Ibáñez B, et al. Lipidomic profiling identifies signatures of metabolic risk. *EBioMedicine* (2020) 51:102520. doi: 10.1016/j.ebiom.2019.10.046

68. Pikó P, Pál L, Szűcs S, Kósa Z, Sándor J, Ádány R. Obesity-related changes in human plasma lipidome determined by the lipidyzer platform. *Biomolecules* (2021) 11(2):326. doi: 10.3390/biom11020326

69. Pietiläinen KH, Sysi-Aho M, Rissanen A, Seppänen-Laakso T, Yki-Järvinen H, Kaprio J, et al. Acquired obesity is associated with changes in the serum lipidomic profile independent of genetic effects-a monozygotic twin study. *PLoS One* (2007) 2(2):e218. doi: 10.1371/journal.pone.0000218

70. Cotte AK, Cottet V, Aires V, Mouillot T, Rizk M, Vinault S, et al. Phospholipid profiles and hepatocellular carcinoma risk and prognosis in cirrhotic patients. *Oncotarget* (2019) 10(22):2161–72. doi: 10.18632/oncotarget.26738

71. Carli F, Pepa GD, Sabatini S, Puig AV, Gastaldelli A. Lipid metabolism in MASLD and MASH: from mechanism to the clinic. *JHEP Rep* (2024) 6(12):101185. doi: 10.1016/j.jhepr.2024.101185

72. Velenosi TJ, Ben-Yakov G, Podszun MC, Hercun J, Etzion O, Yang S, et al. Postprandial plasma lipidomics reveal specific alteration of hepatic-derived diacylglycerols in nonalcoholic fatty liver disease. *Gastroenterology* (2022) 162(7):1990–2003. doi: 10.1053/j.gastro.2022.03.004

73. Horst KWT, Gilijamse PW, Versteeg RI, Ackermans MT, Nederveen AJ, Sel F, et al. Hepatic diacylglycerol-associated protein kinase Cε translocation links hepatic steatosis to hepatic insulin resistance in humans. *Cell Rep* (2017) 19(10):1997–2004. doi: 10.1016/j.celrep.2017.05.035

74. Azbazdar Y, Demirci Y, Heger G, Ipekgil D, Karabicici M, Ozhan G. Comparative membrane lipidomics of hepatocellular carcinoma cells reveals diacylglycerol and ceramide as key regulators of Wnt/β-catenin signaling and tumor growth. *Mol Oncol* (2023) 17(11):2314–36. doi: 10.1002/1878-0261.13520

75. Li Y, Li T, Jin Y, Shen J. Dgat2 reduces hepatocellular carcinoma malignancy *via* downregulation of cell cycle-related gene expression. *Biomed Pharmacother* (2019) 115:108950. doi: 10.1016/j.biopha.2019.108950

76. Safri F, Pickford R, Xu Y, Yang W, Nguyen R, Yuen L, et al. Integrated plasma and tissue lipid profiling demonstrates a distinctive metabolic profile in MAFLD-associated non-cirrhotic hepatocellular carcinoma. *Int J Mol Sci* (2026) 27(13):6060. doi: 10.3390/ijms27136060

77. Tang N, Tang J, Zhang J, Chen H, Yang R. Causal relationship between plasma lipidome and 6 types of cancer: a Mendelian randomization study. *Medicine (Baltimore)* (2025) 104(33):e43900. doi: 10.1097/MD.0000000000043900

78. Morita Y, Sakaguchi T, Ikegami K, Goto-Inoue N, Hayasaka T, Hang VT, et al. Lysophosphatidylcholine acyltransferase 1 altered phospholipid composition and regulated hepatoma progression. *J Hepatol* (2013) 59(2):292–9. doi: 10.1016/j.jhep.2013.02.030

79. Dyall SC, Balas L, Bazan NG, Brenna JT, Chiang N, Souza FC, et al. Polyunsaturated fatty acids and fatty acid-derived lipid mediators: recent advances in the understanding of their biosynthesis, structures, and functions. *Prog Lipid Res* (2022) 86:101165. doi: 10.1016/j.plipres.2022.101165

80. Lee JM, Lee H, Kang S, Park WJ. Fatty acid desaturases, polyunsaturated fatty acid regulation, and biotechnological advances. *Nutrients* (2016) 8(1):23. doi: 10.3390/nu8010023

81. Matsuda M, Kawamoto T, Tamura R. Predictive value of serum dihomo-γ-linolenic acid level and estimated Δ-5 desaturase activity in patients with hepatic steatosis. *Obes Res Clin Pract* (2017) 11(1):34–43. doi: 10.1016/j.orcp.2016.02.004

82. Haycock PC, Borges MC, Burrows K, Lemaitre RN, Burgess S, Khankari NK, et al. The association between genetically elevated polyunsaturated fatty acids and risk of cancer. *EBioMedicine* (2023) 91:104510. doi: 10.1016/j.ebiom.2023.104510

83. Bansal S, Berk M, Alkhouri N, Partrick DA, Fung JJ, Feldstein A. Stearoyl-CoA desaturase plays an important role in proliferation and chemoresistance in human hepatocellular carcinoma. *J Surg Res* (2014) 186(1):29–38. doi: 10.1016/j.jss.2013.07.001

84. Liu HH, Xu Y, Li CJ, Hsu SJ, Lin XH, Zhang R, et al. An SCD1-dependent mechanoresponsive pathway promotes HCC invasion and metastasis through lipid metabolic reprogramming. *Mol Ther* (2022) 30(7):2554–67. doi: 10.1016/j.ymthe.2022.03.015

85. Zhu Y, Gu L, Lin X, Zhou X, Lu B, Liu C, et al. P53 deficiency affects cholesterol esterification to exacerbate hepatocarcinogenesis. *Hepatology* (2023) 77(5):1499–511. doi: 10.1002/hep.32518

86. Fu R, Xue W, Liang J, Li X, Zheng J, Wang L, et al. SOAT1 regulates cholesterol metabolism to induce EMT in hepatocellular carcinoma. *Cell Death Dis* (2024) 15(5):325. doi: 10.1038/s41419-024-06711-9

87. Manolopoulos KN, Karpe F, Frayn KN. Gluteofemoral body fat as a determinant of metabolic health. *Int J Obes (Lond)* (2010) 34(6):949–59. doi: 10.1038/ijo.2009.286

88. An S, Cho S, Yoon JC. Adipose tissue and metabolic health. *Diabetes Metab J* (2023) 47(5):595–611. doi: 10.4093/dmj.2023.0011

89. Lee H, Kubo T, Kono N, Kage-Nakadai E, Gengyo-Ando K, Mitani S, et al. Depletion of mboa-7, an enzyme that incorporates polyunsaturated fatty acids into phosphatidylinositol (PI), impairs PI 3-phosphate signaling in *Caenorhabditis elegans*. *Genes Cells* (2012) 17(9):748–57. doi: 10.1111/j.1365-2443.2012.01624.x

90. Makinoshima H, Umemura S, Suzuki A, Nakanishi H, Maruyama A, Udagawa H, et al. Metabolic determinants of sensitivity to phosphatidylinositol 3-Kinase pathway inhibitor in small-cell lung carcinoma. *Cancer Res* (2018) 78(9):2179–90. doi: 10.1158/0008-5472.CAN-17-2109

91. Nakamura T, Masuda A, Nakano D, Amano K, Sano T, Nakano M, et al. Pathogenic mechanisms of metabolic dysfunction-associated steatotic liver disease (MASLD)-associated hepatocellular carcinoma. *Cells* (2025) 14(6):428. doi: 10.3390/cells14060428

92. Kawashima M, Iwamoto N, Kawaguchi-Sakita N, Sugimoto M, Ueno T, Mikami Y, et al. High-resolution imaging mass spectrometry reveals detailed spatial distribution of phosphatidylinositols in human breast cancer. *Cancer Sci* (2013) 104(10):1372–9. doi: 10.1111/cas.12229

93. Goto T, Terada N, Inoue T, Nakayama K, Okada Y, Yoshikawa T, et al. The expression profile of phosphatidylinositol in high spatial resolution imaging mass spectrometry as a potential biomarker for prostate cancer. *PLoS One* (2014) 9(2):e90242. doi: 10.1371/journal.pone.0090242

94. Wallace C. A more accurate method for colocalisation analysis allowing for multiple causal variants. *Plos Genet* (2021) 17(9):e1009440. doi: 10.1371/journal.pgen.1009440